POLITECNICO DI TORINO

Master's Degree in Environmental and Land Engineering

Master's Degree Thesis

Fed-batch ex-situ biomethanation lab tests: Preliminary technical assessments

Supervisor

Prof. Mariachiara Zanetti

Co-supervisor

Eng. Giuseppe Campo

Candidate

Antonio Busco

Academic Year 2023-2024

To my mother,
whom I always feel
beside me

Abstract

Given the goal of achieving carbon neutrality by 2050 and the widespread adoption of renewable energy sources, it is crucial to examine technologies that reduce environmental impact while maximizing efficiency.

The aim of this work is to develop a fed-batch continuous-stirred tank reactor at laboratory-scale wherein a mesophilic ex-situ biomethanation process occurs. This process utilizes a feedstock comprising digestate from a wastewater treatment plant and a gaseous mixture of H_2/CO_2 in a 4:1 ratio. The work is structured into four parts.

The first part addresses the current status of renewable energy sources in the European Union and the directives related to their utilization, including the Renewable Energy Directive. This is followed by a description of the technologies used in Power-to-Gas (PtG) plants, starting from hydrogen generated from renewable electrolysis and carbon dioxide derived from other processes. Special attention is given to ex-situ biomethanation, focusing on operational principles, various existing configurations, and efficiencies reported in scientific literature.

The second part concerns the experimental section, where tests conducted on the laboratory-scale Continuous Stirred-Tank Reactor (CSTR) are described, with particular focus on parameters such as Methane Evolution Rate (MER) and methane content, which are useful for evaluating the system's operational efficiency. The obtained results include pH values, concentrations of Volatile Fatty Acids (VFAs), macronutrients and biomass present inside the reactor. The methodologies employed in the various analyses are reported in the appendices in the fourth part.

The third part presents the conclusions drawn from the conducted tests, focusing

on the efficiency of the system's operation, also in comparison with systems reported in the literature. In particular, it is observed that the system is able to achieve high MER values, up to 8.57 L CH_4/L/d, but accompanied by hydrogen content values not sufficiently low to allow direct injection into the natural gas grid, according to the limits set by technical regulations. Reducing the partial pressure of carbon dioxide and hydrogen could be an option to address this issue. Furthermore, it emerges that the analysed system is thermally self-sufficient. This aspect is important for evaluating its implementation also on real scale in various contexts, such as within a wastewater treatment plant.

Acknowledgements

A heartfelt thank you to Professor Mariachiara Zanetti, for her professionalism and kindness from the very beginning of this thesis work.
I also wish to express my gratitude to Engineer Giuseppe Campo, for his constant availability and support throughout the entire journey.
I also thank Engineer Alberto Cerutti for the great assistance provided to me, particularly in laboratory activities.
A huge thank you also to my father, my brother, and my friends, near and far, for supporting me during my studies and throughout this work, and for accompanying me to the achievement of this important milestone.

Contents

List of Figures

List of Tables

Part I

Introduction

Chapter 1

Renewable energy and fuels

1.1 Renewable Energy in Europe

Renewable energy, derived from inexhaustible or regenerating sources, stands out as one of the most relevant contemporary issues. It represents a key pathway towards achieving the goals set forth in the 2015 Paris Agreement, including limiting the increase in global average temperature and ensuring a reduction in greenhouse gas emissions. In 2009, through Directive 2009/28/EC [6], the European Commission called upon member states to develop infrastructure for transmission, distribution, and storage to maximize the utilization of renewable energy production. Presently, within the European Union, renewable sources contribute predominantly to electricity production, followed by fossil fuels and nuclear energy. According to the data presented in Figure 1.1, it is observed that in 2022, the net electricity production amounted to 2641 TWh, with the following breakdown:

- Nearly 40% from renewable sources;
- 38.6% from fossil fuels, with natural gas being the most prominently utilized;
- Over 20% from nuclear energy.

With the introduction of the Green Deal in 2019 by the European Commission, the primary objective is to achieve climate neutrality by 2050, meaning to make the EU neutral in terms of greenhouse gas emissions. To this end, the production

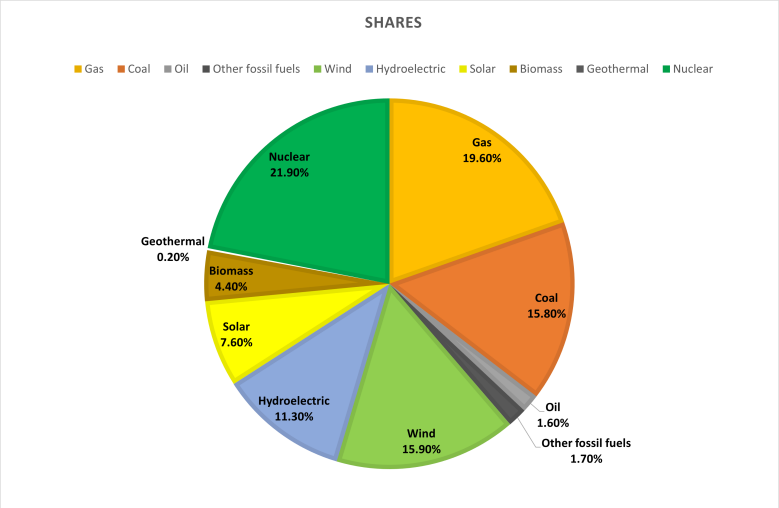

Figure 1.1: Shares of different fuels in European Union in 2022 [9]

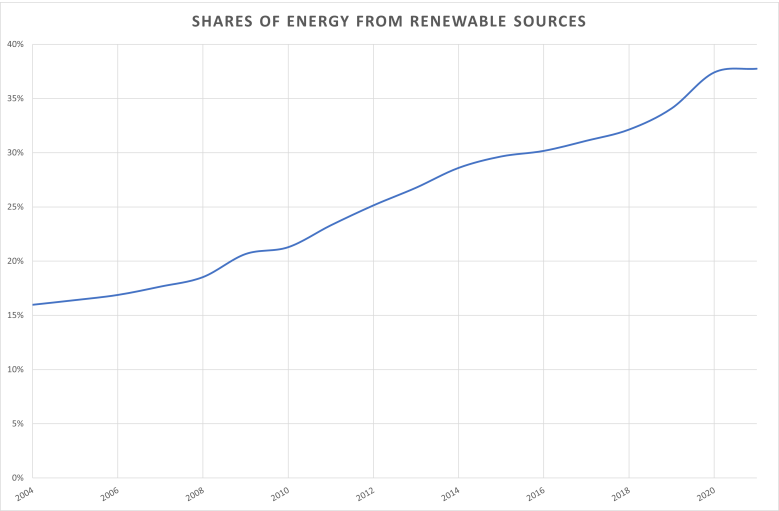

Figure 1.2: Shares of electricity from renewable sources in EU 2004-2022. [9]

of electricity from renewable sources is expected to increase over time, as highlighted in the graph in Figure 1.2: the production, which represented 15.9% in 2004, has more than doubled by 2022 and it is expected to further increase. In the Figure 1.4, estimates for the projected energy mix in the years 2030 and 2050 are depicted. Each country displays a diversified energy mix, shaped by various interconnected factors. It emerges as the outcome of a balance influenced by natural

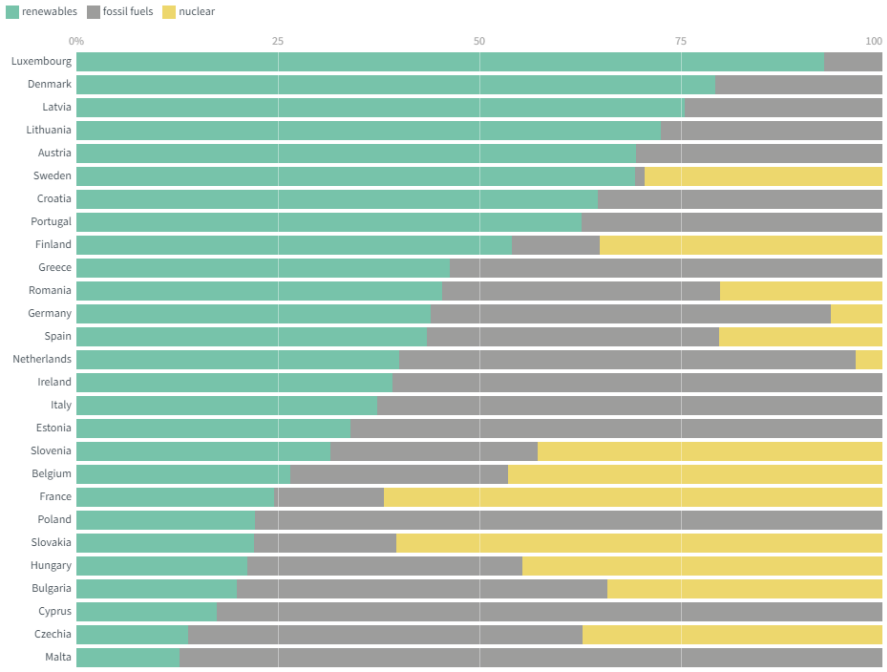

Figure 1.3: Energy mixes in the various EU countries. [9]

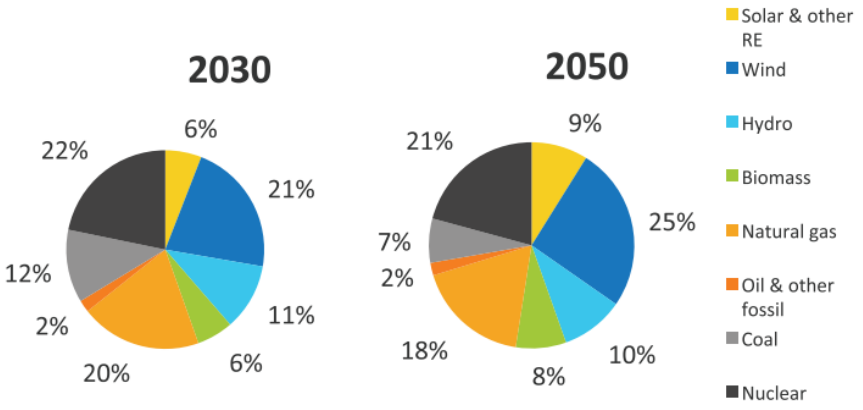

Figure 1.4: Estimated energy mix in 2030 and 2050. [25]

resources, government policies and incentives, existing infrastructure, geographical and climatic conditions, resource price trends, environmental objectives, and foreign dependency. In Figure 1.3, a bar chart illustrates the proportions of renewable energies, fossil fuels, and nuclear energy utilized for electricity generation

in the 27 EU countries. Italy stands out for the absence of nuclear energy usage but exhibits a percentage of 37% in the utilization of renewable sources.
It is important to highlight how peaks in production and consumption rarely coincide, necessitating the evaluation of methods for storing energy surpluses. Between 2012 and 2016, the surplus value recorded in the European Network of Transmission System Operators averaged 39 TWh annually [25]. Additionally, energy generated from solar and wind sources requires transmission methods to reach areas with higher demand. The production of Renewable Fuels of Non-Biological Origin can present a viable option to address these issues.

1.2 Renewable Fuels of Non-Biological Origin

In addition to the prominent goal of achieving carbon neutrality by 2050 and the need to store energy surpluses, it is crucial to consider that the depletion of fossil fuels, anticipated as a consequence of elevated energy demand, and the energy crisis due to the Russia-Ukraine conflict, contribute to an ever-increasing energy price.
A key factor that can be employed to address these issues may be represented by the use of *Renewable Fuels of Non-Biological Origin* (*RFNOs*), which are liquid and gaseous fuels, distinct from biofuels or biogas, with their energy content derived from renewable sources other than biomass. According to the *Renewable Energy Directive II* [7], RFNOs can contribute to reduce carbon emissions, encourage decarbonization, primarly in the transport sector and foster innovation, growth, and employment in the Union's economy, as well as reduce dependence on energy imports.
With the subsequent revision of the Renewable Energy Directive (*RED III*) [8], Renewable Fuels of Non-Biological Origin are more extensively discussed, specifying that they should be regarded as renewable energy regardless of the sector in

which they are consumed. Indeed, they represent a crucial means to increase the share of renewable energy in sectors that, in the long term, should primarily rely on liquid and gaseous fuels, such as industrial applications and heavy transport. In specific terms, Member States guarantee that the share of RFNOs utilized for both final and non-final energy purposes constitutes a minimum of 42% of the hydrogen employed for final and non-final energy applications by 2030 and increases to 60% by 2035.

A viable option to consider is the utilization of renewable electricity as a fuel source. This has led to the emergence of the *Power-to-Fuel* (PtF) system, which involves the conversion of energy, particularly electricity, generated from renewable sources into zero-carbon synthetic fuels with the aim of replacing products linked to fossil fuels. The term 'Fuel' refers to the synthetic hydrocarbon fuels produced and the systems can be diversified as *Power-to-Gas* (PtG) or *Power-to-Liquid* (PtL), depending on the type of final product obtained. Fuels that are produced using hydrogen from water, employing sustainable electricity as the principal power source, are known as *electrofuels* or *e-fuels* [14]. Specifically, electrofuels hold a key advantage as energy storage carriers, facilitating the storage of energy generated from renewable sources during periods of surplus. This is particularly significant due to the intermittent and discontinuous nature of renewable sources. The main synthetic fuels include power-to-hydrogen (PtH_2), power-to-methane ($PtCH_4$), power-to-methanol ($PtCH_3OH$), and power-to-ammonia ($PtNH_3$) [28]. In the Figure 1.5, an overview of available renewable PtF technologies is presented.

1.2.1 E-Hydrogen

This Power-to-Hydrogen system involves production of *e-hydrogen* (or *green hydrogen*) through the utilization of electricity generated from renewable sources. The method employed for this conversion is known as electrolysis. It entails the

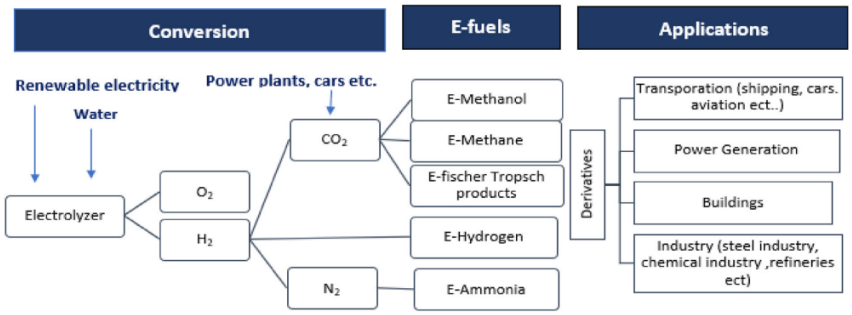

Figure 1.5: E-fuels and their applications [28]

splitting of water molecules as represented by the Equation 1.1:

$$\mathrm{H_2O\,(l)} \longrightarrow \mathrm{H_2(g)} + \frac{1}{2}\,\mathrm{O_2\,(g)} \tag{1.1}$$

The electrolysis process takes place using suitable electrolyzers, the operation of which is elucidated in Paragraph 2.2.

1.2.2 E-Ammonia

Ammonia is synthesized through the Haber-Bosch process under conditions of temperature ranging between 400 and 500 °C and pressure between 100 and 450 bar, in the presence of an iron-based catalyst, according to the Equation 1.2:

$$3\,\mathrm{H_2} + \mathrm{N_2} \longrightarrow 2\,\mathrm{NH_3} \quad \Delta H_r = -91.8\,\mathrm{kJ/mol} \tag{1.2}$$

It finds various applications, such as a raw material for fertilizer production and a clean fuel for transportation and power generation. Moreover, it serves as an excellent carbon-free energy carrier for hydrogen storage. The term *"e-ammonia"* is used when referring to the compound resulting from the synthesis of nitrogen derived from the air, using specific separation methods such as membrane separation and pressure swing adsorption, and hydrogen produced from renewable

sources [28].

1.2.3 E-Methanol

Methanol can be produced through catalytic hydrogenation of carbon dioxide under conditions of temperature ranging from 200 to 300 °C and pressure between 50 and 100 bar, in the presence of zinc or copper oxide as a catalyst, following the Equation 1.3.

$$CO_2 + 3\,H_2 \longrightarrow CH_3OH + H_2O \quad \Delta H_r = -49.2\,\mathrm{kJ/mol} \tag{1.3}$$

It exhibits various applications, being a widely employed solvent and also serving as a fuel in transportation, electricity production, and wastewater treatment. It can be derived from fossil fuels or renewable energy sources, taking the form of *biomethanol* or *e-methanol*. *Biomethanol* is derived from biomass gasification or biogas produced in landfills or from anaerobic digesters, while *e-methanol* is produced from captured carbon dioxide and renewable hydrogen [28].

1.2.4 E-Methane

The synthesis of methane generally occurs according to the Equation 1.4, which is called *methanation*.

$$4\,H_2 + CO_2 \longrightarrow 2\,H_2O + CH_4 \quad \Delta H_r = -165\,\mathrm{kJ/mol} \tag{1.4}$$

Methane plays a pivotal role as a clean fuel due to its minimal CO_2 emissions when compared to other hydrocarbon fuels. *E-methane* is synthesized through a Power-to-Methane (PtM) system, as shown in Figure 1.6. Methanation process proves advantageous for several reasons. Notably, hydrogen is considered a promising

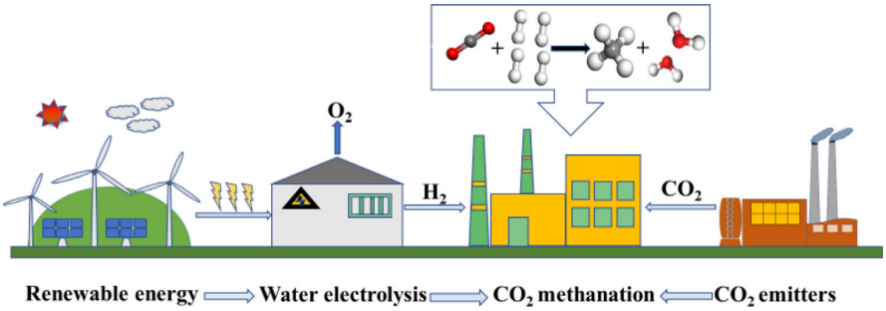

Figure 1.6: E-Methane synthesis [21]

energy carrier but requires expensive infrastructure for storage and modern technologies for its use as a fuel due to its low density. In contrast, methane can be directly injected into existing infrastructures, such as natural gas reserves and the gas network, and can be used directly as a transport fuel. Additionally, methane has a higher volumetric heating value (36 MJ/m^3) compared to hydrogen (10.88 MJ/m^3). Finally, it is important to highlight the usefulness of PtM process in reducing CO_2 emissions. [34]

One of the areas in which methanation can be applied is represented by the pro-

Table 1.1: Typical biogas composition [24]

Molecule	**Concentration in the biogas**
Methane (CH_4)	55-65%
Carbon dioxide (CO_2)	35-45%
Hydrogen sulfide (H_2S)	0.02-0.2%
Vapor (H_2O)	saturation
Hydrogen (H_2), Ammonia (NH_3) Oxygen (O_2), Molecular Nitrogen (N_2), siloxanes	in traces

duction of biogas through anaerobic digestion of biomass or waste. Anaerobic digestion is a process involving the decomposition of organic raw materials such

as organic wastes, animal manure, and agricultural byproducts, favored by the presence of anaerobic bacteria. The typical composition of the produced biogas is reported in the Table 1.1. However, to be injected into the natural gas grid or used in co-generation plants for combined heat and power production, it needs to undergo an upgrading process. Through this process, the removal of CO_2 and other impurities takes place, resulting in a stream primarily composed of CH_4, referred to as "*biomethane*". The captured CO_2, on the other hand, can undergo a methanation process with hydrogen, leading to the production of what is termed "*e-methane*".

Chapter 2

Power-to-Methane

2.1 Introduction to PtM system

The Power-to-Methane system, also referred to as Renewable Power Methane (RPM), involves the following phases:

- *Water electrolysis*, producing hydrogen using renewable sources;
- *Capture of CO_2* from the original source, ensuring it reaches sufficient purity for the process;
- *Methanation*, based on the reaction between hydrogen and carbon dioxide, which can occur chemically or biologically.

A schematic representation of a PtM system is provided in Figure 2.1.

2.2 Water electrolysis

The process of water electrolysis defines the synthesis of hydrogen from water, as expressed in Equation 1.1 outlined in Paragraph 1.2.1. It shows an overall reaction which results from two electrochemical reactions shown in Equation 2.1 and Equation 2.2.

$$2\,H_2O + 2\,e^- \longrightarrow 2\,OH^- + H_2 \tag{2.1}$$

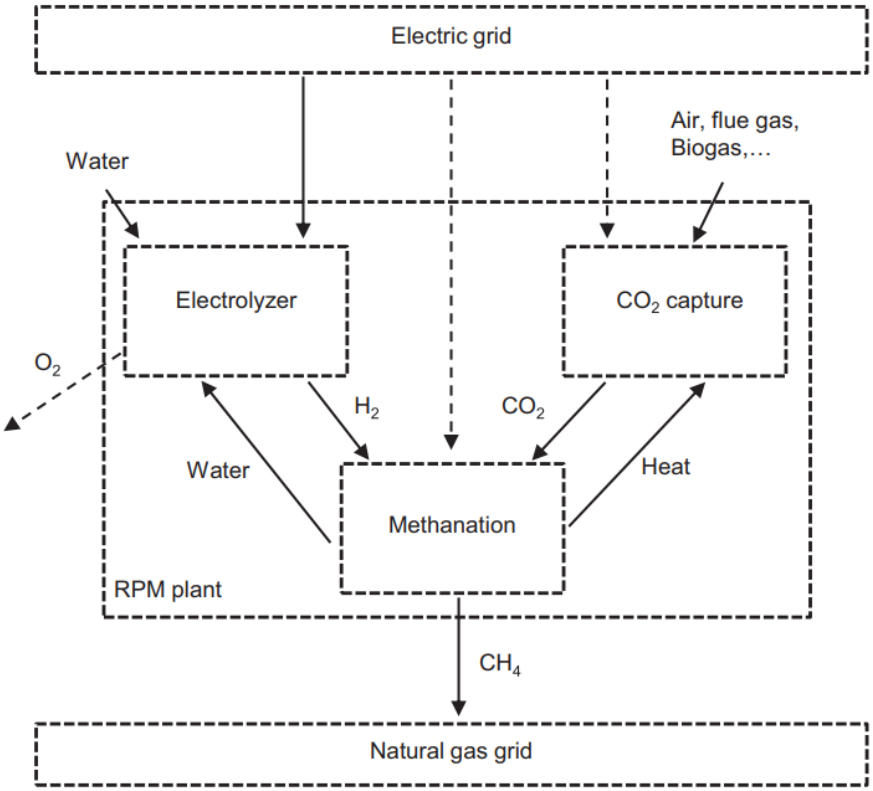

Figure 2.1: Renewable Power Methane system [25]

$$2\,OH^- \longrightarrow \frac{1}{2}\,O_2 + H_2O + 2\,e^- \tag{2.2}$$

The Equation 2.1 represents a reduction reaction occurring at the negatively charged cathode, while Equation 2.2 depicts an oxidation reaction taking place at the positively charged anode.

Three distinct types of electrolyzers are available for utilization: alkaline electrolyzer, polymer electrolyte membrane and solid oxide electrolyzer.

2.2.1 Alkaline electrolyzer (AEC)

Alkaline electrolyzers are the most widely employed, particularly for large-scale hydrogen production. They use an alkaline electrolyte composed of an aqueous

solution of potassium hydroxide (KOH) or sodium hydroxide (NaOH), with two electrodes immersed within it, separated by a separator as illustrated in Figure 2.2. They typically operate at temperatures ranging from 60 to 80 °C and can operate at atmospheric pressure or elevated pressures.

The main advantage, especially for pressurized electrolyzers, lies in the production of compressed hydrogen that does not require additional energy for injection into the grid. However, a significant drawback is associated with high maintenance costs due to corrosion caused by the electrolyte used [28].

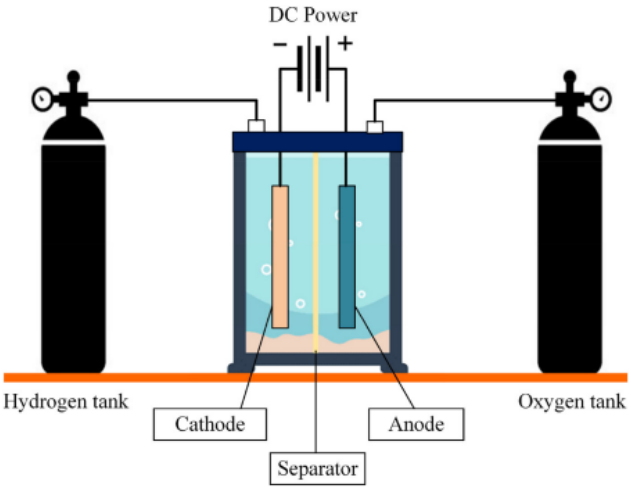

Figure 2.2: AEC electrolyzer [32]

2.2.2 Polymer electrolyte membrane (PEM)

It is designed to operate at temperatures below 80 °C. As shown in Figure 2.3, it is primarily composed of a solid polymer material membrane, which facilitates the selective conduction of electrons during the electrolysis process, allowing the passage of the produced hydrogen while impeding that of oxygen ions. On both sides of the membrane, layers of catalyst, typically platinum, are applied, constituting the electrodes known as Membrane Electrode Assemblies. The electrodes play a

pivotal role by promoting reactions both at the anode and cathode during the electrochemical process. Gas diffusion layers are positioned on both sides of the electrodes to facilitate the interaction of hydrogen and oxygen in electrochemical reactions, thereby enhancing the efficiency of the process. Finally, on the outer sides of the electrodes, there are separator plates or bipolars, made of conductive material. These plates serve various functions, including providing structural support to maintain the integrity of the stack, conducting electricity between different cells, and creating channels for the passage of gases.

In comparison to AECs, they yield hydrogen with enhanced purity and exhibit a broader operational range and increased flexibility. However, the drawback is linked to higher investment costs, stemming from the utilization of noble metals as catalysts [28].

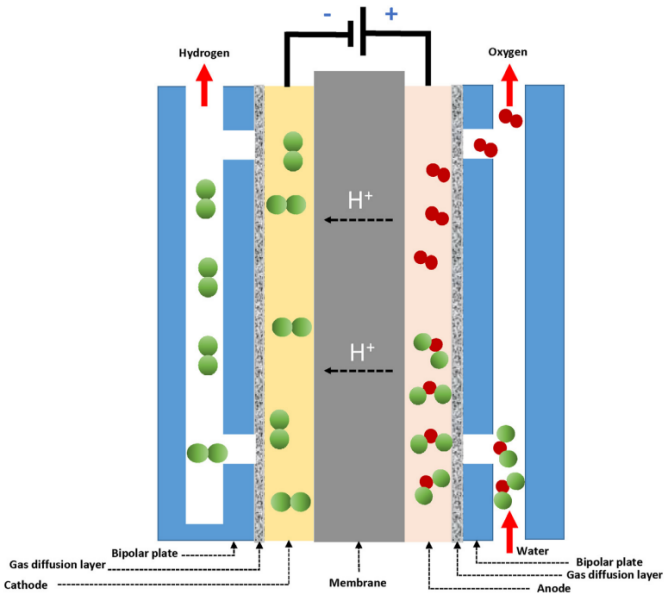

Figure 2.3: The cross sectional of PEM electrolyzer [29]

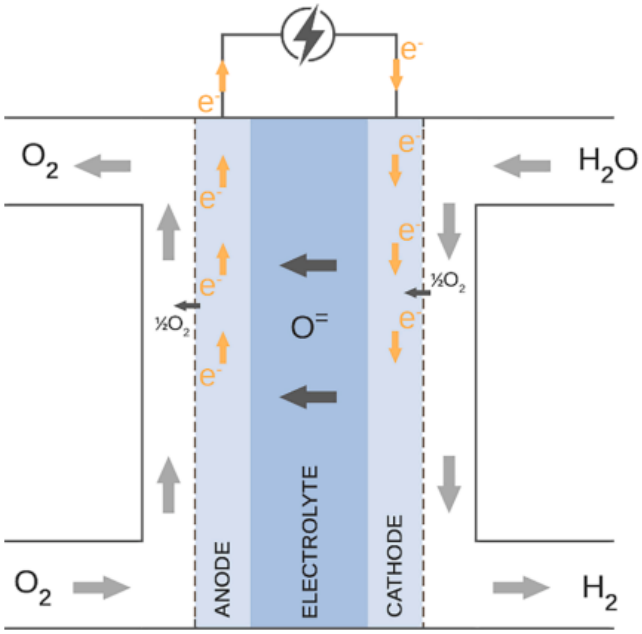

Figure 2.4: The working principles of solid oxide electrolysis. [27]

2.2.3 Solid Oxide Electrolyzer (SOE)

As shown in Figure 2.4, Solid Oxide Electrolyzer (SOE) is composed of a solid electrolytic membrane, typically made of ceramics and an oxygen-conducting material such as yttria-stabilized zirconia or gadolinium-doped cerium oxide.
By applying an electrical voltage to the membrane, it selectively allows the passage of oxygen ions, which migrate towards the anode, where the separation of oxygen from water molecules occurs. The SOE operates at high temperatures, generally ranging between 600 and 1000 °C. This temperature range optimizes the conductivity of oxygen ions through the solid membrane, contributing to the overall efficiency of the process.
The distinctive advantage of the SOE system lies in its lower electricity consumption due to higher conversion efficiency compared to other systems. However, a significant drawback is associated with the rapid degradation of materials caused

by the high working temperatures [28].

2.3 CO_2 capture

For the PtM process, carbon dioxide is required in addition to hydrogen. The Table 2.1 illustrates possible processes, whose exhaust gases can be utilized as sources for CO_2. Among the most relevant for this study is biogas, a gaseous mixture primarily composed of methane, accounting for 55-65%, and carbon dioxide, constituting 35-45%.

There are four different technologies that can be employed to obtain high-purity CO_2 from various sources, as shown in Figure 2.5 [12, 22]: absorption, adsorption, membrane separation and cryogenic distillation.

Table 2.1: Potential CO_2 sources for PtM [12]

Sectors	CO_2 **sources**	CO_2 **concentration in exhaust gas**
Biomass processes	Biomass fermentation	15-50%
	Biogas upgrading	≈100%
	Bioethanol production	≈100%
Power generation plants	Natural gas combustion	3-5%
	Petroleum combustion	3-8%
	Coal combustion	10-15%
Industrial processes	Cement production	14-33%
	Iron and steel production	20-30%
	Ethylene oxide production	≈100%
Environment	Ambient air	≈0.04%

2.3.1 Absorption

Based on the type of absorbent employed, the following distinction can be made:

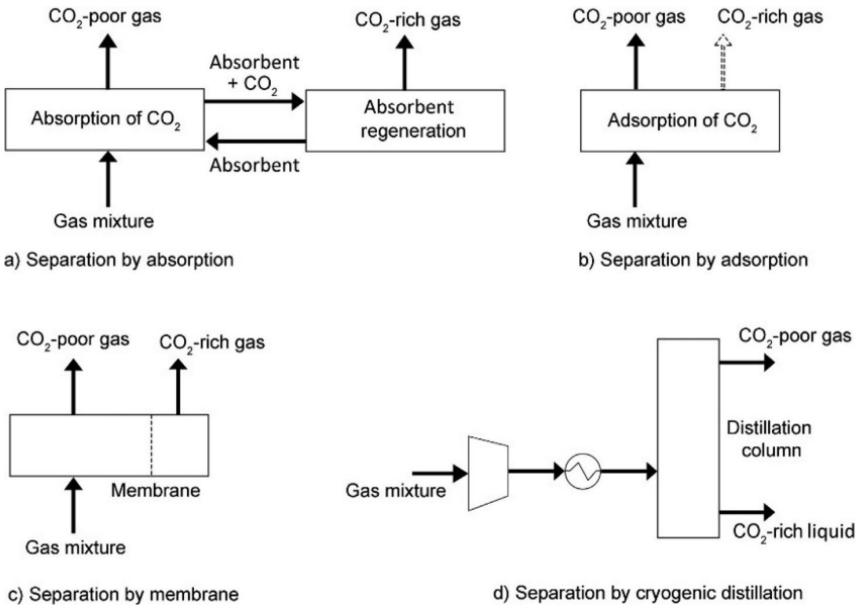

Figure 2.5: CO_2 capture technologies [12]

- *Physical Absorption:* It is based on the difference in solubility of exhaust gases within liquid absorbents (e.g., alcohols), aiming to create a solution. After the absorption process, the absorbent is decompressed releasing CO_2 and recycled in the process.

- *Chemical Absorption:* This method, more used, is based on the reaction of CO_2 with the absorbent. A commonly employed reagent is organic amine solution, composed of monoethanolamine (MEA), diethanolamine (DEA) and methyldiethanolamine (MDEA). After the process, the product is heated to regenerate the absorbent, which can be recycled.

It is shown in Figure 2.5a.

2.3.2 Adsorption

The mechanism is based on the electrostatic or van der Waals forces that arise between the solid porous medium, defined as the *adsorbent*, and carbon dioxide, defined as the *adsorbate*. As shown in Figure 2.5b, CO_2, under conditions of low temperature and high pressure, is captured on the surface of the adsorbent; subsequently, heating and depressurization are employed for its release. Among the commonly utilized adsorbent materials, two noteworthy examples are:

- Activated carbon, which is characterized by a high specific surface area (up to 1700 m^2/g), but with adsorption capacity strongly influenced by CO_2 partial pressure;
- Zeolites, known for their high adsorption capacity which is significantly affected by temperature and presence of vapor.

2.3.3 Membrane separation

Through the use of membranes, it is possible to achieve gas separation under pressure by exploiting the distinct molecular sizes of various substances, as depicted in Figure 2.5c and Figure 2.6.

The driving force facilitating this process is the difference in partial pressure of CO_2 between the two sides of the membrane. Two main types of membranes are distinguished:

- Polymeric (organic) membranes: Widely utilized, but characterized by low selectivity for carbon dioxide.
- Inorganic membranes: More efficient in separation, yet underutilized due to their high associated costs.

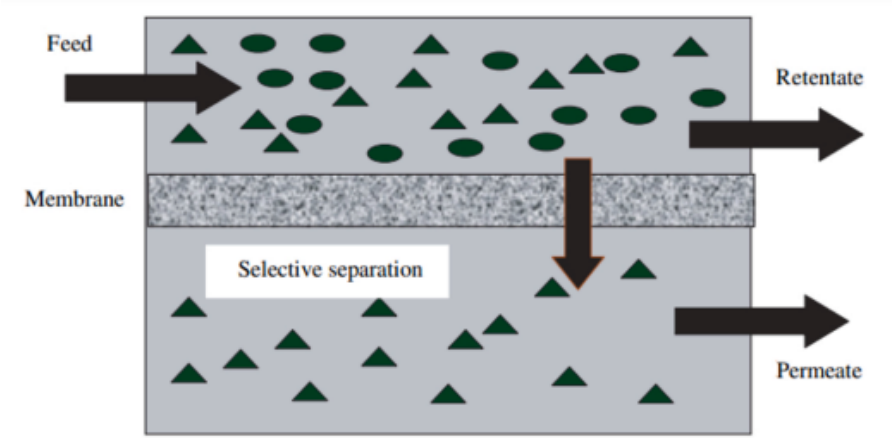

Figure 2.6: Gas separation membrane [10]

2.3.4 Cryogenic distillation

The method, depicted in Figure 2.5d, relies on the difference in boiling points of various substances present in exhaust gases. The input is subjected to low temperatures and high pressures to ensure the liquefaction of gases. In a suitable distillation column, the separation of CO_2 from the remaining components is then carried out. In general, it is used for the separation of other gases such as nitrogen and oxygen, requiring substantial amounts of energy [12].

2.4 Chemical Methanation

Chemical methods, categorized based on the driving force of the process, include thermocatalytic, electrocatalytic, and photocatalytic processes.
While methanation is a straightforward reaction, the mechanism can be intricate due to the simultaneous occurrence of other reactions that may impact the efficiency of the process. The methanation reaction is exothermic, implying that thermodynamically, at low temperatures and high pressures, there is a high conversion of CO_2 and a high selectivity for methane, as illustrated in the graphs in

Figure 2.7. However, at temperatures exceeding 450°C, methane selectivity diminishes significantly due to the initiation of the reverse water-gas shift (RWGS) process, leading to the formation of CO as a byproduct according to the Equation 2.3.

$$CO_2 + H_2 \rightarrow CO + H_2O \tag{2.3}$$

The formation of byproducts is further favored at higher pressures.
The catalytic process involves the synthesis of methane through the Sabatier reaction, as expressed in Equation 1.4, and takes place under conditions of temperature ranging from 250 to 400 °C and pressure between 5 and 50 bar. [28] The catalyst employed in the process consists of active metals (such as Ni, Co, Ru, or Rh) loaded on a metal oxide support (such as Al_2O_3, SiO_2, CeO_2, ZrO_2) or zeolites. Chemical methanation can utilize not only a stream consisting mainly of CO_2 but

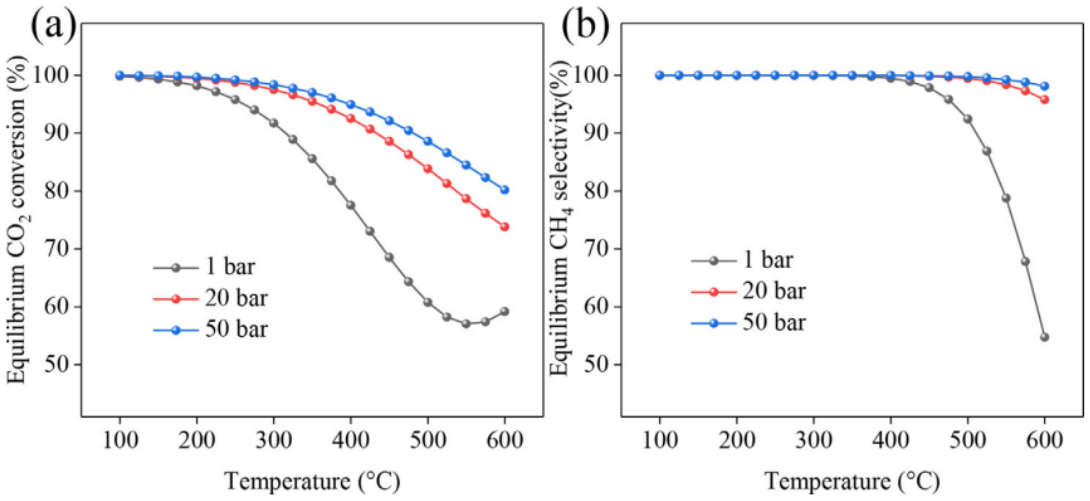

Figure 2.7: Effect of temperature and pressure on the chemical methanation process [22]

also biogas, performing a *direct biogas methanation* as shown in the Figure 2.8.

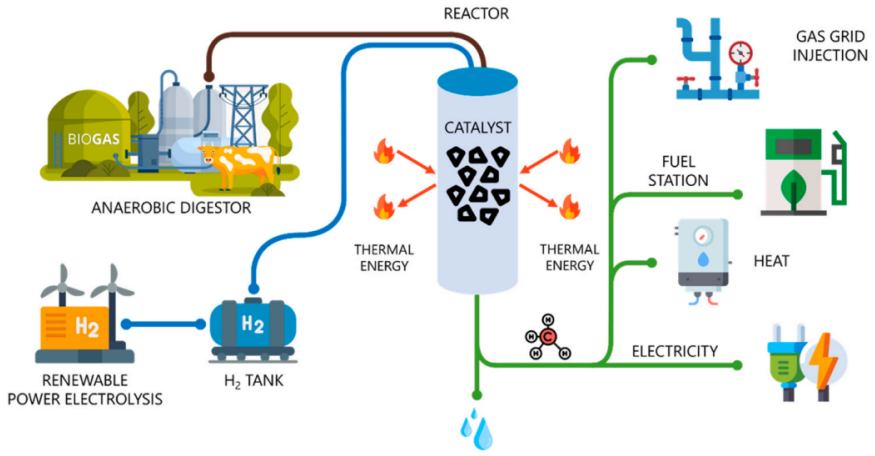

Figure 2.8: Direct biogas methanation [36]

2.5 Biomethanation

Biomethanation is a biological process in which hydrogen from renewable sources and carbon dioxide present in biogas are converted into methane by hydrogenotrophic metanogenic microorganisms. It can take place in various reactor configurations and in two different modes, as shown in Figure 2.9: *in-situ* or *ex-situ*.

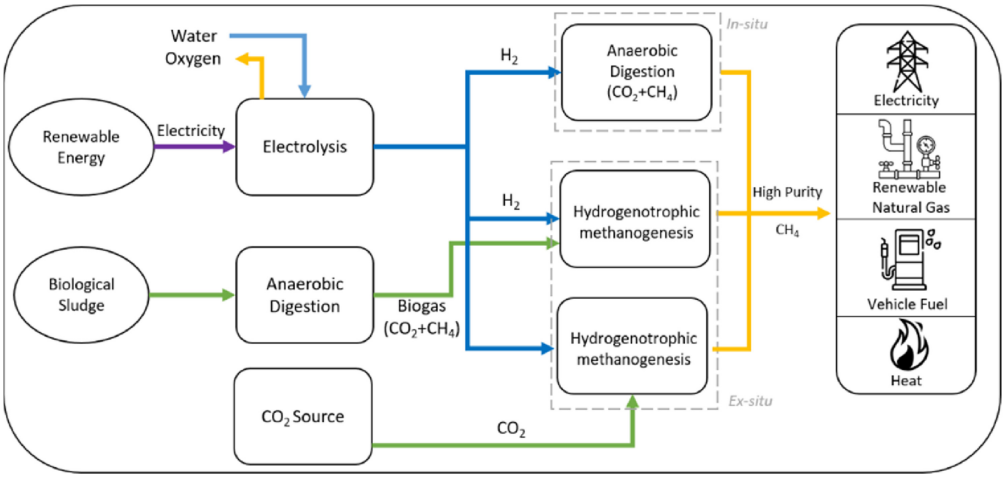

Figure 2.9: In-situ and ex-situ reactors [18]

2.5.1 Efficiency parameters

To assess the efficiency of the reactors, it is imperative to proceed with the analysis and comparison of certain parameters, as outlined below in the paragraph [13].

Methane Evolution Rate

The Methane Evolution Rate (MER) serves as a straightforward approach for assessing system performance. It quantifies the volume of methane produced over a specified timeframe relative to the reactor volume and is calculated using Equation 2.4:

$$\text{MER} = \frac{Q_{\text{CH}_4,\text{out}} - Q_{\text{CH}_4,\text{in}}}{V_R} \left[\frac{L}{L_{\text{sludge}} d}\right] \tag{2.4}$$

Here, $Q_{\text{CH}_4,\text{out}}$ (L/d) represents the volumetric flow rate of methane exiting the reactor, and $Q_{\text{CH}_4,\text{in}}$ (L/d) denotes the volumetric flow rate of methane entering. V_R is the volume of sludge in the reactor (L_{sludge}).

Retention Time

The Retention Time (RT) is a parameter that expresses the residence time of the fluid within the reactor. It is defined as the ratio of the reactor volume V_R (L) to the daily fluid flow rate Q (L/d) through it, as expressed in Equation 2.5.

$$RT = \frac{V_R}{Q} \; [d] \tag{2.5}$$

Efficiency of H_2 utilization

The efficiency of H_2 utilization (η_{H_2}) provides information regarding the hydrogen consumption during the process.

$$\eta_{H_2} = \frac{\text{H}_2 \text{ loading rate - H}_2 \text{ rate in output gas}}{\text{H}_2 \text{ loading rate}} \cdot 100 \tag{2.6}$$

The calculation can be performed using Equation 2.6, where "H_2 loading rate" (L/(L$_R$ d)) represents the incoming hydrogen rate, and "H_2 rate in output gas" (L/(L$_R$ d)) represents the rate of hydrogen in the outgoing gas.

Methane yield

The methane yield (Y_{CH_4}) provides information regarding the methane production yield from the incoming hydrogen.

$$Y_{CH_4} = \frac{\text{Output gas rate} \cdot x_{CH_4,\,out}}{H_2 \text{ loading rate}} \tag{2.7}$$

The calculation can be performed using Equation 2.7, where "Output gas rate" (L/(L$_R$ d)) represents the total rate of effluent gas and "$x_{CH_4,\,out}$" is the CH_4 molar fraction in the effluent gas.

2.5.2 Reactor configurations

The Figure 2.10 illustrates the various possible configurations that can be employed during the biomethanation process.

Continuous Stirred Tank Reactor (CSTR)

This reactor, depicted in Figure 2.10a, is a continuous-flow reactor consisting of a tank fed with a constant flow of material and equipped with an agitation system to ensure uniform intensive properties in space. It is the most widely used in this type of process due to its simplicity, effective mixing, and suitability for large-scale facilities. Additionally, it is cost-effective. The primary determinant of biomethanation efficiency resides in the H_2 gas-liquid mass transfer rate ($K_L\alpha$). Therefore, the principal objective involves minimizing the dimensions of H_2 and CO_2 bubbles through the optimization of the agitation system, impeller design,

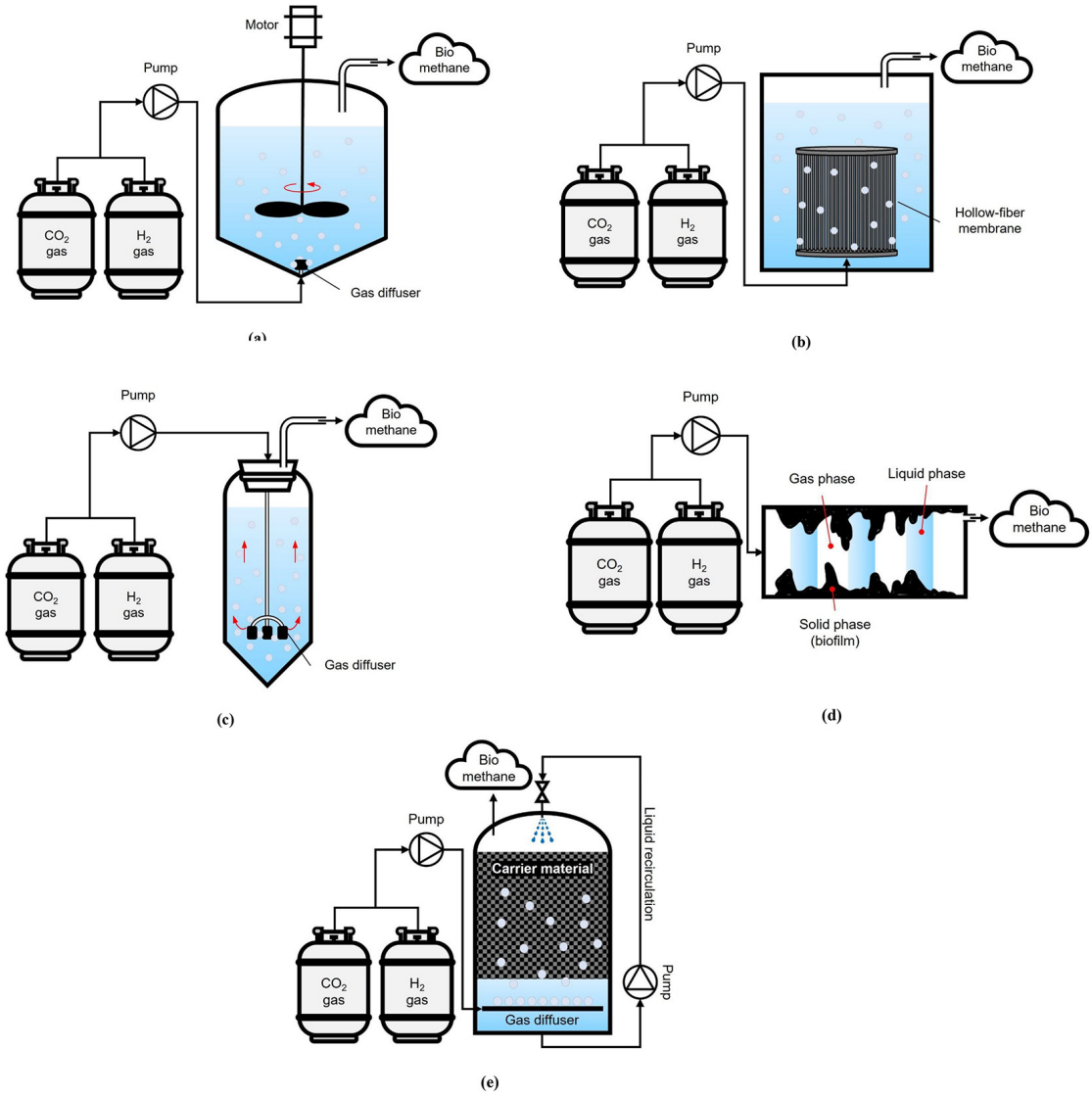

Figure 2.10: Various reactor configurations for the injection of H_2 and CO_2 in the methanation process.[34]

and gas diffusion.

On a laboratory scale, reactors reaching speeds of up to 1500 rpm are employed, whereas on an industrial scale, speeds typically reach 60 rpm.[35]

Membrane Reactor

This reactor, in Figure 2.10b, consists of a hollow fiber membrane through which the gaseous substrate passes and diffuses into the liquid phase, making it available for microorganisms. The membrane is composed of various fibers, allowing gas to pass through small pores and enabling instantaneous gas-liquid mass transfer. The main disadvantage is the formation of biofilm by microorganisms, which can clog the pores and reduce the efficiency of the system.

Up-flow and Bubble Column Reactor

Characterized by a high height-to-depth ratio, these reactors feature ceramic or stainless steel gas diffusers to reduce the size of hydrogen bubbles. They are depicted in Figure 2.10c.

Plug-flow Reactor (PFR)

As shown in Figure 2.10d, it consists of a polyvinyl-chloride (PVC) tube packed with polyethylene wheels to immobilize microorganisms and suspended on a frame to create vertical loops. The gaseous substrate (H_2 and CO_2) continuously passes through the tube.

Trickle Bed Reactor (TBR)

It comprises a fixed bed filled with porous packing material with a high specific surface area where microorganisms are immobilized. Unlike other reactors, it is filled with gas instead of liquid, as depicted in Figure 2.10e. A liquid medium trickles down to provide nutrients to the microbes, forming a liquid film around the biofilm on the surface of the packing material. This reactor demonstrates the highest efficiency in methane production due to the creation of the biofilm-gas-liquid phase interaction that enhances the mass transfer rate of hydrogen. Furthermore,

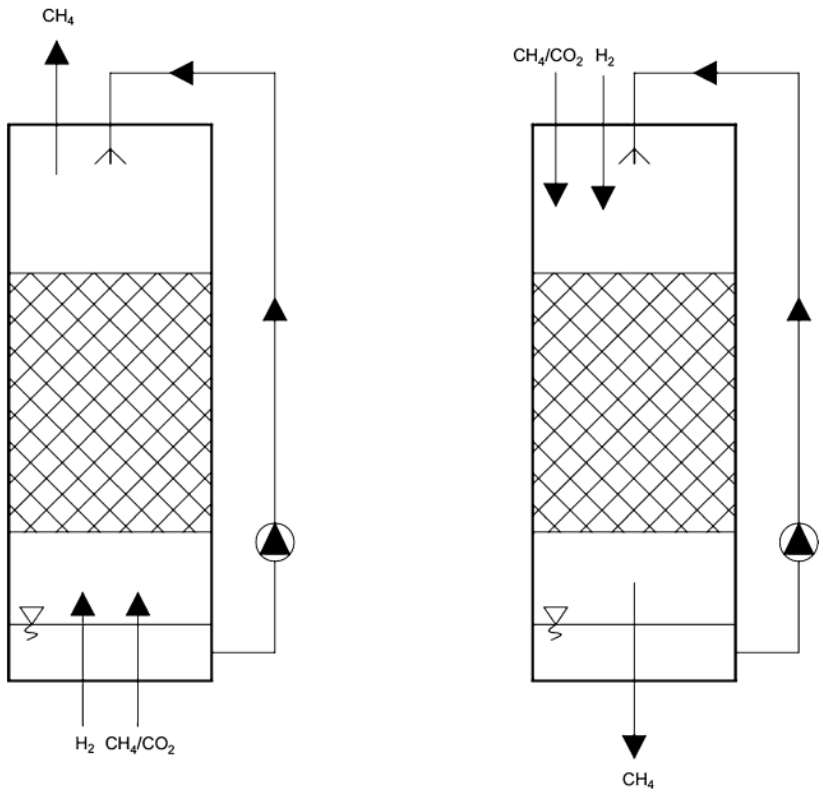

Figure 2.11: TBR concurrent (a) and countercurrent (b) configurations [33]

it does not require large amounts of energy to ensure continuous mixing or bubbling. As shown in Figure 2.11, it can be in two possible configurations: concurrent (or up-flow gas configuration) or countercurrent(or down-flow gas configuration), depending on whether the substrate enters from the bottom or the top of the reactor.

2.5.3 Hydrogen mass transfer

One of the most critical aspects in developing a technically and economically viable biomethanation process on an industrial scale is H_2 gas-liquid mass transfer.

Specifically, gas-liquid mass transfer constrains the reaction rate of biomethanation, as the lower solubility of H_2 in the aqueous solution leads to reduced availability for microorganisms. The mass transfer process can be elucidated through

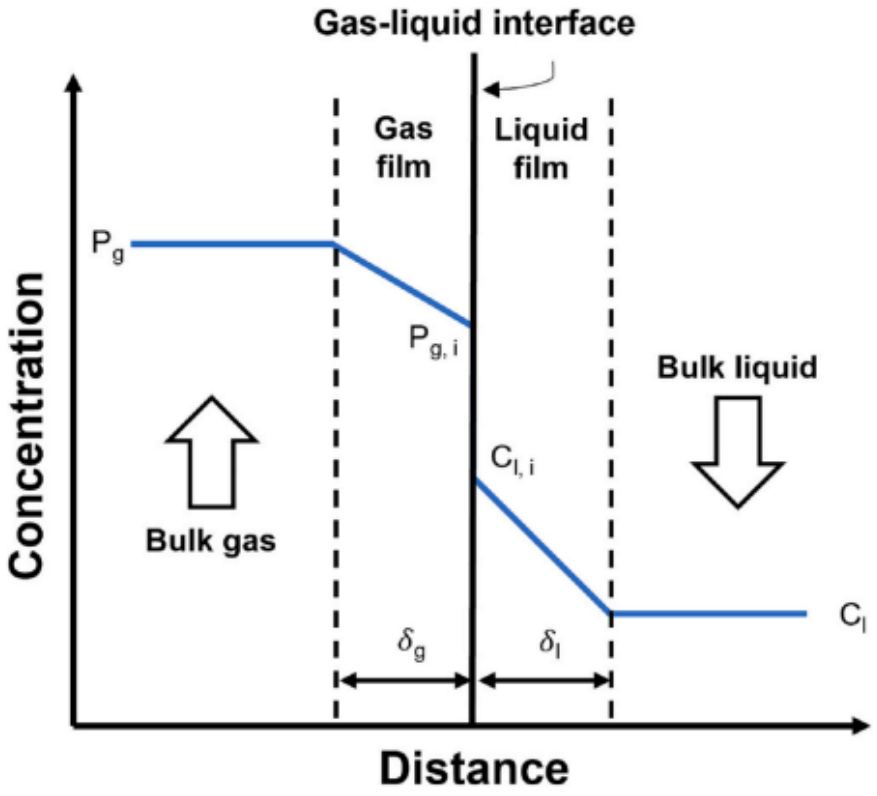

Figure 2.12: Two-film theory [34]

the *two-film theory*, as shown in Figure 2.12. Here, P_g is the gas partial pressure in the bulk gas phase; C_l is the dissolved gas concentration in the bulk liquid; $P_{g,i}$ and $C_{l,i}$ are, respectively, the gas partial pressure and the dissolved gas concentration at the gas-liquid interface; δ_g and δ_l are, respectively, the gas and liquid boundary layer thicknesses. [34]

Both the bulk gas and the bulk liquid exhibit homogeneous concentrations of the gaseous solute but are not in equilibrium with each other. Molecular diffusion

occurs across the stagnant layers of the liquid and gas phases adjacent to the interface between gas and liquid. These two layers represent the resistances to the solute's passage from the bulk gas to the bulk liquid. Steady-state conditions are assumed to be achieved, where the gas flux from bulk gas to bulk liquid equals the flux of gas occurring in the individual films.

In particular, the mass transfer process occurs in multiple stages, as highlighted in Figure 2.13: the gas reaches the gas-liquid interface; once past the interface, it diffuses through the liquid film surrounding the gas bubble; subsequently, it traverses the surrounding liquid and then permeates through the liquid film surrounding the microbial cells; it then crosses the liquid-solid interface and the cell envelope, ultimately reaching the site where the biochemical reaction takes place. Utilizing Fick's law, the mass transfer of hydrogen from the gaseous phase to the liquid phase can be mathematically described through the Equation 2.8:

$$R_t = 22.4 \cdot K_L\alpha(H_{2g} - H_{2l}) \tag{2.8}$$

In this relation, R_t is the rate of substrate utilization by biomass [mol/L/h], 22.4 represents the volume of 1 mol of gas at standard temperature and pressure [L/mol], $K_L\alpha$ is the gas-liquid mass transfer coefficient [h^{-1}], while $(H_{2g} - H_{2l})$ is the concentration gradient [mol/L]. This gradient represents the difference between the concentrations of H_2 in the gas phase and that dissolved in the liquid phase. The $K_L\alpha$ value is influenced by the reactor configuration, specifically the stirring speed, gas recirculation, and the presence of gas diffusers and packing materials.

Stirring

Among the crucial aspects, the impeller design and agitation speed play a significant role in reducing the size of H_2 gas bubbles and generating shear forces to decrease the thickness of stagnant liquid at the gas-liquid interface. Overall, this

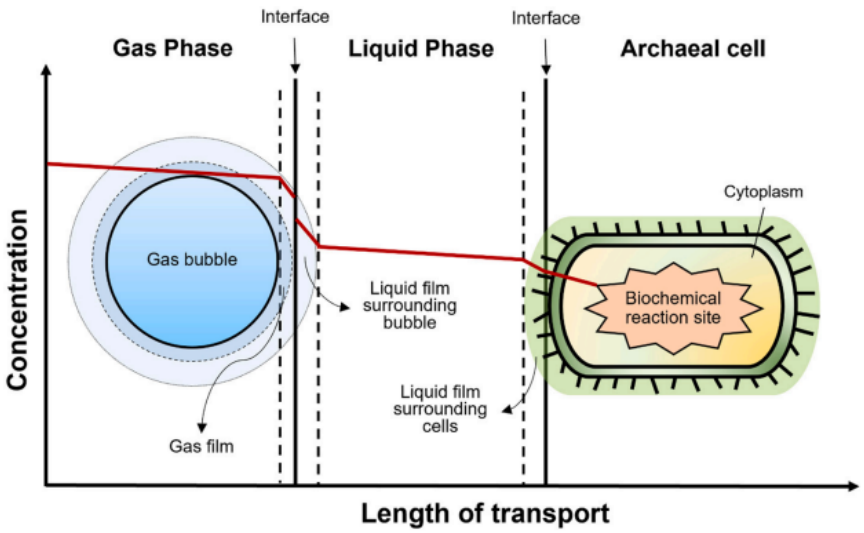

Figure 2.13: H_2 mass transfer in different stages [34]

promotes mass transfer.

The effect of agitation can be described using Van't Riet correlations, as reported in Equation 2.9, based on experiences of O_2 gas-liquid mass transfer in aqueous solutions:

$$K_L\alpha = A \cdot \left(\frac{Pw}{V}\right)^B \cdot v_s^C \tag{2.9}$$

Here, Pw is the power consumed for agitation (W), V is the reactor volume, v_s is the superficial gas velocity (which is the volumetric gas flow rate per unit of cross-sectional area of the reactor), and A, B, and C are empirical constants.

Intense mixing results in higher energy consumption but ensures an enhancement in mass transfer.

Gas recirculation

Gas recirculation also leads to an increased mass transfer of H_2 between gas and liquid, as there is a longer interaction time between the two phases, providing greater opportunities for methanogens to interact with the gas. In particular,

Bassani et al. [2] observed that doubling the headspace gas recirculation in thermophilic up-flow reactors results in a 36% increase in $K_L\alpha$ and an enhancement in CH_4 purity.

Gas diffuser

Gas diffusers facilitate the dispersion of gases into small bubbles, ensuring easier and faster dissolution in water. Accompanied by stirring, these instruments lead to a further increase in $K_L\alpha$ value due to the enhanced interaction between the two phases and the formation of a turbulent flow, which further breaks down the bubbles into smaller sizes. The materials used for diffuser construction can include ceramic, fish stone, and stainless steel.

Packing materials

Packing materials serve as a beneficial support for microorganisms, promoting their contact with gas and increasing $K_L\alpha$ value. However, it is important to limit the presence of dead zones. As evidence of this, Kougias et al. [17] observed that in up-flow reactors, the presence of packing materials resulted in higher hydrogen consumption efficiency and increased methane content compared to values obtained in the absence of packing materials under the same operating conditions. These materials can be classified into natural ones (such as vermiculite shales, granular perlite, crushed clay) and commercial ones (such as glass rings and polyurethane foam).

2.5.4 Microbial communities in biological methanation systems

The Figure 2.14 illustrates the primary reactions that can occur during the process of biomethanation. The biometanation process can occur through two distinct

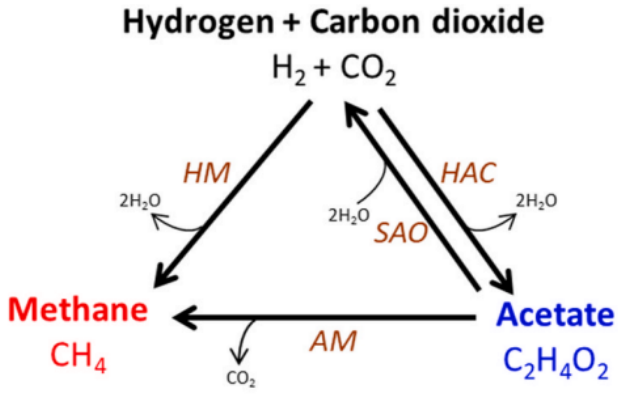

Hydrogenotrophic methanogenesis (HM):	$4H_2 + CO_2 \rightarrow CH_4 + 2H_2O$
Homoacetogenesis (HAC):	$4H_2 + 2CO_2 \rightarrow C_2H_4O_2 + 2H_2O$
Acetoclastic methanogenesis (AM):	$C_2H_4O_2 \rightarrow CH_4 + CO_2$
Syntrophic acetate oxidation (SAO):	$C_2H_4O_2 + 2H_2O \rightarrow 4H_2 + 2CO_2$

Figure 2.14: Main biological reactions in biomethanation process [19]

pathways:

- *Hydrogenotrophic Methanogenesis Pathway*: This involves the direct conversion of carbon dioxide into methane by hydrogenotrophic methanogenic archaea, utilizing external H_2 as the electron donor, as illustrated in Equation 1.4.

- *Indirect Pathway*: In this route, CO_2 is transformed into acetate by homoacetogenic bacteria through the Wood-Ljungdahl pathway. Subsequently, acetate is converted into methane by acetoclastic methanogenic archaea, as depicted in Equations 2.10 and 2.11.

$$4H_2 + 2CO_2 \rightarrow CH_3COOH + 2H_2O \quad \Delta G^{\circ\prime} = -104.5\,\mathrm{kJ/mol} \tag{2.10}$$

$$CH_3COOH \rightarrow CH_4 + CO_2 \quad \Delta G^{\circ\prime} = -31.0\,\mathrm{kJ/mol} \tag{2.11}$$

It is important to note that the second pathway necessitates a higher energy

expenditure than the first, as a greater energetic input is required to maintain two distinct microbial groups rather than just one. However, the concentration of H_2 serves as a parameter significantly influencing the equilibrium in the process. On one hand, the addition of external hydrogen promotes the growth of both hydrogenotrophic methanogens (HM) and homoacetogens (HAC). Particularly, Taspekos et al. [37] observed that under various pH conditions (neutral or alkaline) and pressure, the permissive H_2 partial pressure is consistently higher for the homoacetogenic pathway than for the methanogenic one. On the other hand, however, H_2 may inhibit syntrophic acetogens (responsible for the degradation of propionate and butyrate into acetate) and syntrophic acetate oxidizers (SAO).
Regarding temperature conditions, Laguillaumie et al. [19] observed, through the analysis of microbial consortia behavior in successive batches, that at a temperature of 35°C, no detection of acetate occurs, and *Methanobacterium* HM prevails over HAC. Conversely, at a temperature of 25 °C, simultaneous production of acetate and methane occurs, facilitated by the coexistence of HMs and *Acetobacterium* HAC.
Concerning pH, Garcia et al. [11] observed that, in a survey involving 68 methanogenic species, most of these species demonstrated optimal growth within the pH range of 6 to 8. In particular, the optimal range was identified to be between 6.6 and 7.3 [23].
In Table 2.15, the optimal temperature and pH characteristics for the growth of some methanogenic species are reported. In the biometanation process, the most relevant microorganisms are hydrogenotrophic methanogens, including *Methanobacterium, Methanoculleus, Methanomicrobium*, and *Methanothermobacter*. Acetoclastic methanogens (AM), such as *Methanosarcina*, are present in lower abundance.
It is important to emphasize that the use of mixed adapted cultures is consistently

Species	Substrate	Optimal temperature (°C)	Optimal pH range
Methanobacterium bryantii	H_2/CO_2	37	6.9-7.2
Methanobacterium formicicum	H_2/CO_2, formate	37-45	6.6-7.8
Methanobacterium thermoalcaliphium	H_2/CO_2	58-62	8.0-8.5
Methanothermobacter thermoautotrophicum	H_2/CO_2	65-70	7.0-8.0
Methanothermobacter wolfeii	H_2/CO_2	55-65	7.0-7.5
Methanobrevibacter smithii	H_2/CO_2, formate	37-39	-
Methanobrevibacter ruminantium	H_2/CO_2, formate	37-39	-
Methanothermus fervidus	H_2/CO_2, formate	83	< 7
Methanothermococcus thermolithotrophicus	H_2/CO_2, formate	65	-
Methanococcus voltae	H_2/CO_2, formate	35-40	6.0-7.0
Methanococcus vannielli	H_2/CO_2, formate	65	7.0-9.0
Methanomicrobium mobile	H_2/CO_2, formate	40	6.1-6.9
Methanolacinia paynteri	H_2/CO_2	40	7.0
Methanospirillum hungatei	H_2/CO_2, formate	30-40	-
Methanosarcina acetivorans	Methanol, acetate	35-40	6.5
Methanosarcina barkeri	H_2/CO_2, methanol, methylamines, acetate	35-40	5.0-7.0
Methanosarcina mazei	Methanol, methylamines, acetate	30-40	6.0-7.0
Methanosarcina thermophile	H_2/CO_2, methanol, methylamines, acetate	50	6.0-7.0
Methanococcoides methylutens	Methanol	42	7.0-7.5
Methanosaeta concilii (soehngenii)	Acetate	35-40	7.0-7.5
Methanosaeta thermophila	Acetate	55-60	7.0

Figure 2.15: Characteristics of methanogenic species [40]

preferred over pure cultures for several reasons:

- Microbial communities exhibit greater resilience.
- Sterilization is unnecessary, avoiding associated additional costs.
- Expenses related to the potential inoculation of large quantities of pure cultures in large-scale facilities are circumvented.

2.5.5 In-situ biomethanation

Through in-situ configuration, as shown in Figure 2.16, exogenous hydrogen from renewable sources is injected into the biogas reactor and reacts with endogenous carbon dioxide produced from anaerobic digestion to be converted into methane by the presence of Methanogenic Archaea. In this process, biomethanation takes place in the same reactor where the degradation of organic material occurs.
Various factors must be taken into account.

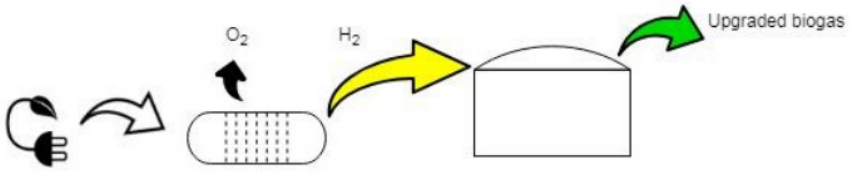

Figure 2.16: In-situ configuration. [4]

First, to obtain a high methane recovery, it is imperative to exert complete control over operational parameters. Among these, pH assumes a pivotal role, with a threshold value of 8.5 for both thermophilic and mesophilic conditions. Beyond this value, there is a consequential inhibition of methanogenesis. The escalation of pH may be attributed to the dissolution of CO_2 in the aqueous phase, as shown

in Equation 2.12.

$$CO_2 + H_2O \longrightarrow H^+ + HCO_3^- \tag{2.12}$$

As evidence of this, Wang et al. [39] observed that in-situ methanation in a CSTR housing sewage sludge at 37°C is able to achieve an H_2 conversion efficiency of 96%, methane recovery of 98.9%, and CO_2 removal of 99%, only if pH control is implemented.

Moreover, elevated concentrations of H_2 (>10 Pa) present another critical aspect, potentially leading to the inhibition of volatile fatty acids (VFA) oxidation. This inhibition manifests in the accumulation of various byproducts, including lactate, ethanol, propionate, butyrate, and notably acetate. The ensuing excessive acidity further exacerbates the situation, resulting in a discernible decrease in acetoclastic methanogenic activity.

Furthermore, the solubilization of H_2 in the liquid phase emerges as a critical factor influencing reactor performance. This underscores the importance of a thoughtful approach to reactor design, recognizing that the dynamics of H_2 solubility have implications for the overall efficiency and effectiveness of the system. In essence, these interconnected considerations emphasize the need for a comprehensive understanding and strategic integration of various factors in the pursuit of optimized biomethanation processes. [1]

The main advantage of in-situ configuration lies in the fact that it does not require additional infrastructure; the disadvantage is that a rigorous control system for parameters is necessary.

2.5.6 Ex-situ biomethanation

In the ex-situ configuration, as depicted in Figure 2.17, carbon dioxide from an external source, along with hydrogen, is injected into an anaerobic reactor for methane production by hydrogenotrophic microorganisms. The main drawback

of this approach is represented by the fact that it is necessary to introduce an additional reactor, which entails inevitable and non-negligible costs for investment and maintenance [1], but it can offer several advantages compared to the in-situ method:

- Ensures stability in the initial anaerobic digestion process, as the biomethanation phase takes place in a separate reactor.
- Simplifies the biochemical process by eliminating the need to degrade organic substances; the input consists directly of CO_2.
- Is not dependent on biomass.
- Allows for the use of various sources of CO_2, not limited to biogas.

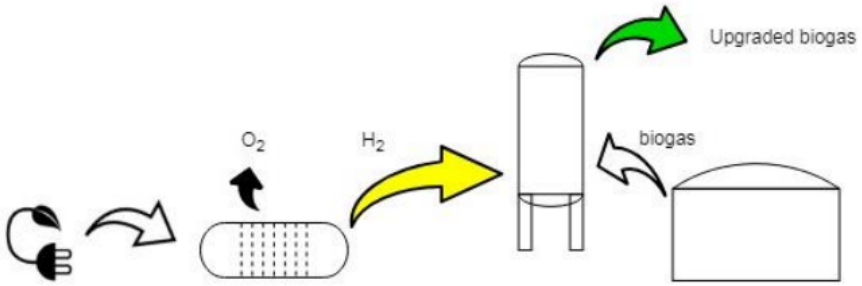

Figure 2.17: Ex-situ configuration. [4]

The last advantage can allow achieving higher volumetric methane production rates with shorter gas retention time compared to in-situ approaches, which, on the other hand, need to ensure sufficient time for both the anaerobic digestion process and methanation. Indeed, Voelklein et al. [38] noted that, in thermophilic condition at 55°C, a higher MER was achieved in a CSTR in ex-situ configuration, reaching $3.7\,\mathrm{L/(L_{sludge}\,d)}$ with 96% methane content, compared to the in-situ configuration value, equal to $2.5\,\mathrm{L/(L_{sludge}\,d)}$.

However, it is interesting to note that Miehle et al. [26], working under mesophilic conditions at 37°C in a CSTR, achieved a MER of $2.21\,\mathrm{L/(L_{sludge}\,d)}$ with a methane

Table 2.2: Anaerobic batch tests in CSTR [18]

Types of reactor	T (°C)	H_2:CO_2	% CH_4
Batch	37	1:1	23
		2:1	42
		3:1	58
		4:1	69
	55	1:1	24
		2:1	45
		3:1	63
		4:1	73

content of 99%. This MER value, in comparison to the evidence presented by Voelklein et al. [38], appears lower, likely due to the lower operating temperatures.

Moreover, in relation to operational conditions, Kozak et al.[18] assessed the average concentration of CH_4 produced in a CSTR through anaerobic batch tests. The gas retention time was maintained at 24 hours, while variations were introduced in temperature conditions (mesophilic and thermophilic) and the concentration ratio of H_2:CO_2 at the inlet. The results, presented in Table 2.2, indicate that higher temperatures and an increased concentration ratio lead to higher methane production. Additionally, Rachbauer et al. [31] observed a higher MER even in a trickle-bed reactor under a stoichiometric ratio of H_2:CO_2 equal to 4. Therefore, it can be stated that this condition is optimal in any case, regardless of the type of reactor employed.

2.5.7 Pilot scale and industrial scale

Conducting tests on a pilot scale allows for a clearer understanding of the actual efficiency of the reactors, enabling a more comprehensive evaluation of the options to be implemented on an industrial scale.

Optimal values are reported in the Table 2.3 and are based on the evidence of Jonson et al. [16], using two pilot TBRs installed on-site at Nature Energy Holsted A/S in Denmark, converting raw biogas from an industrial-scale digester. The system is depicted in Figure 2.18, where V1, V2, and V3 represent three valves regulating the incoming biogas flow. The experience was conducted both in parallel (V1 and V2 open, V3 closed) and in series (V1 and V2 closed, V3 open).

Currently, several companies are manufacturing industrial-scale reactors. Among

Table 2.3: Pilot-scale TBRs tests [16]

Operating Configuration	**MER ($Nm^3/(m^3\ d)$)**	**CH_4 Content (%)**
Series	10.6	97.4
Parallel	9.44	95.7

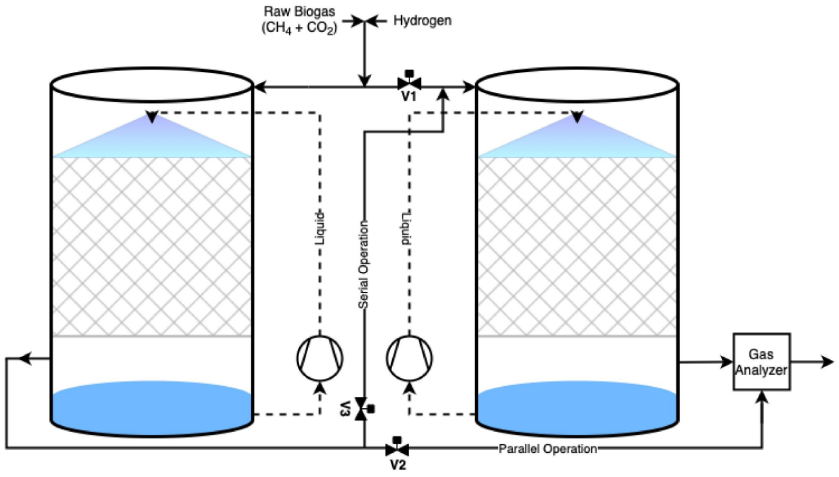

1

Figure 2.18: System configuration of the two TBRs. [16]

these, *PlanEnergi* stands out, having implemented two technologies in Germany and Denmark, as listed in Table 2.4 along with their respective operating conditions.

The goal is to ensure the biomethanation of biogas using hydrogen produced

Table 2.4: PlanEnergi biogas methanation technologies [30]

Location	**CH_4 (%)**	**H_2 (%)**	**CO_2 (%)**	**Methanation efficiency (%)**	**P (bar)**	**T (°C)**
Avedore, Denmark	>98	<2	<1	84	9	63
Allendorf, Germany	>95	<3	<3	75-80	5	40

through electrolysis. The compositions obtained from different plants are suitable for direct injection into the natural gas grid.

Another company is *Electroarchea*, which has implemented three Biocat reactors in Denmark [20]. These reactors comprise TBRs filled with a biocatalyst patented by the University of Chicago. Operating at temperatures of 63°C and a pressure of 10 bar, they ensure a methanation efficiency of 100%, utilizing CO_2 from biogas and green H_2 from electrolysis.

2.5.8 Heat production

An important aspect to consider is the exothermicity of the methanation reaction, as highlighted in Equation 1.4. Engelbrecht et al. [5] conducted an analysis of a laboratory-scale TBR designed to operate in both up-flow and down-flow configurations, as shown in Figure 2.11, using a substrate flow rate of $3\,\mathrm{NL}_{\mathrm{CO}_2}/(L_R\,\mathrm{d})$. Achieving a methane content of $97.4 \pm 0.3\%$, an increase in temperature was observed in both cases, reaching reactor core temperatures of 78 °C in the up-flow configuration (Figure 2.19A) and 74 °C in the down-flow configuration (Figure 2.19B). These temperature values constitute a plateau, at which the heat losses from the reactor are in balance with the metabolic heat production. The inability to overcome these plateaus is attributed to the hypothesis that there is self-regulation by microorganisms to counteract the generated thermal stress.

Therefore, temperature control is necessary to ensure that the biomethanation

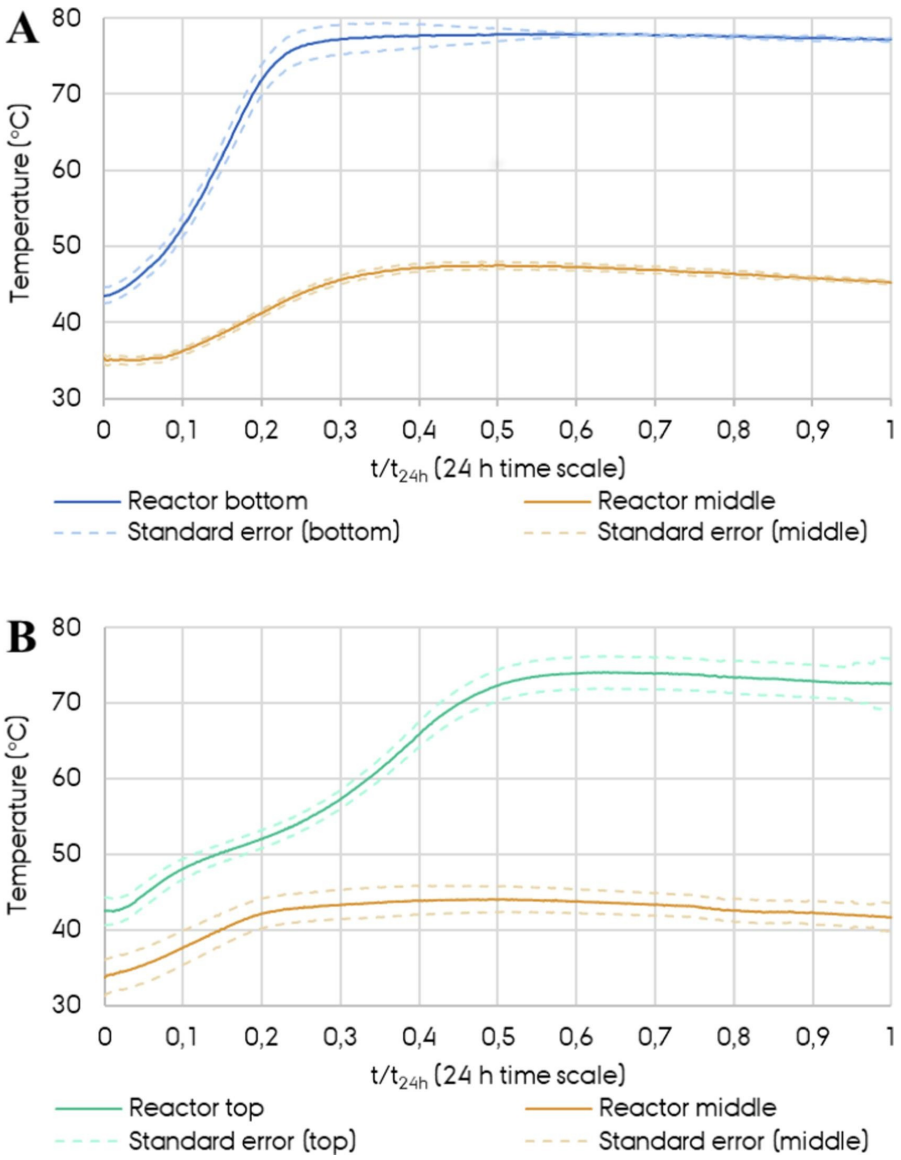

Figure 2.19: Temperature profiles and standard errors of reactor inlet and mid sections for the up-flow gas configuration (A) and the down-flow gas configuration (B) [5]

process occurs under optimal conditions. However, it is important to note that the amount of heat produced is not negligible: there is a production of 12.2 MJ/Nm^3 of transformed CO_2. This form of energy can thus be employed for other activities, improving overall energy efficiency.[5]

Consequently, metabolic heat can present an opportunity for the improvement of ex-situ biomethanation process and may serve as an additional incentive to employ this technology in conjunction with other large-scale activities, such as wastewater treatment plants, utilizing biogas from sludge digestion as a feedstock.

Part II

Experimental Section

Chapter 3

Laboratory tests

3.1 Materials and Methods

It has been decided to proceed with the laboratory-scale implementation of a continuous stirred reactor to assess its efficiency in methane production during the ex situ biomethanation process under mesophilic conditions. The system operates under fed-batch conditions, meaning it has an open inlet and a closed outlet.
A photo of the entire system is shown in Figure 3.1 .

As inoculum, digested sludge from the wastewater treatment plant in Castiglione Torinese (TO), managed by the company SMAT S.p.A., has been utilized. Within the digestate, there are biomass components conducive to methane production, particularly hydrogenotrophic and acetoclastic methanogens. Overall, three tests were conducted, and the process configurations are illustrated in Figure 3.2 and Figure 3.3.

In all configurations, the system consisted of a 2.6 L Schott bottle serving as the reactor (R), within which a specified volume of digestate was placed. The bottle was equipped with an electric resistance that heated the reactor, ensuring, through a thermostat control (TIC), that the temperature was maintained consistently at 38 °C. Complete mixing within the bottle was facilitated by a SEAFLO membrane pump with adjustable speed, allowing for the recirculation of the mixed liquor. This was drawn from the bottom of the reactor and reintroduced above the liquid level to ensure enhanced mixing.

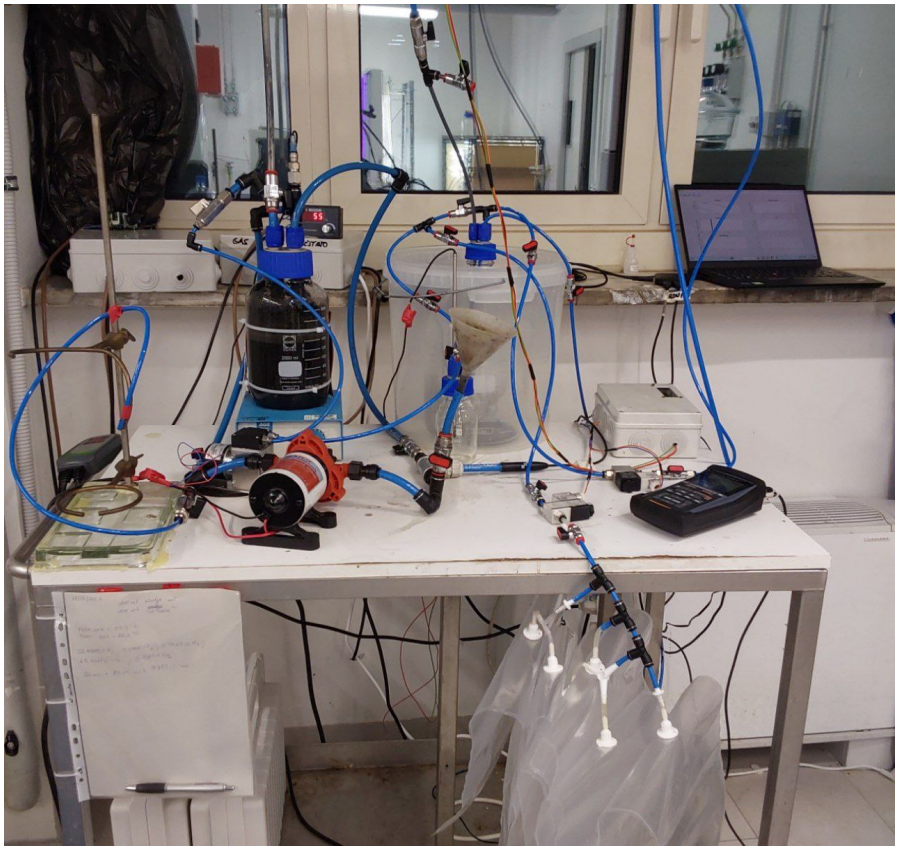

Figure 3.1: Ex-situ biomethanation at laboratory-scale

Within the system, a mixture of H_2/CO_2 in a 4:1 ratio was introduced from a certified cylinder, serving the purpose of providing substrate to hydrogenotrophic microorganisms, essential for methane production. To further enhance mixing and ensure greater contact between substrate and biomass, the mixture was pumped into the lower part of the reactor using an additional membrane pump. The gaseous mixture was then collected from the reactor and directed into another 6 L Schott bottle, functioning as a gasometer (G1), where a pressure indicator and controller (PIC) were installed.

Particularly, the operation took place under pressure conditions ranging from 1400 mbar to 1100 mbar. After filling the available volume with the H_2/ CO_2 gas mixture and reaching the predetermined maximum pressure, the electrovalve EV1 was

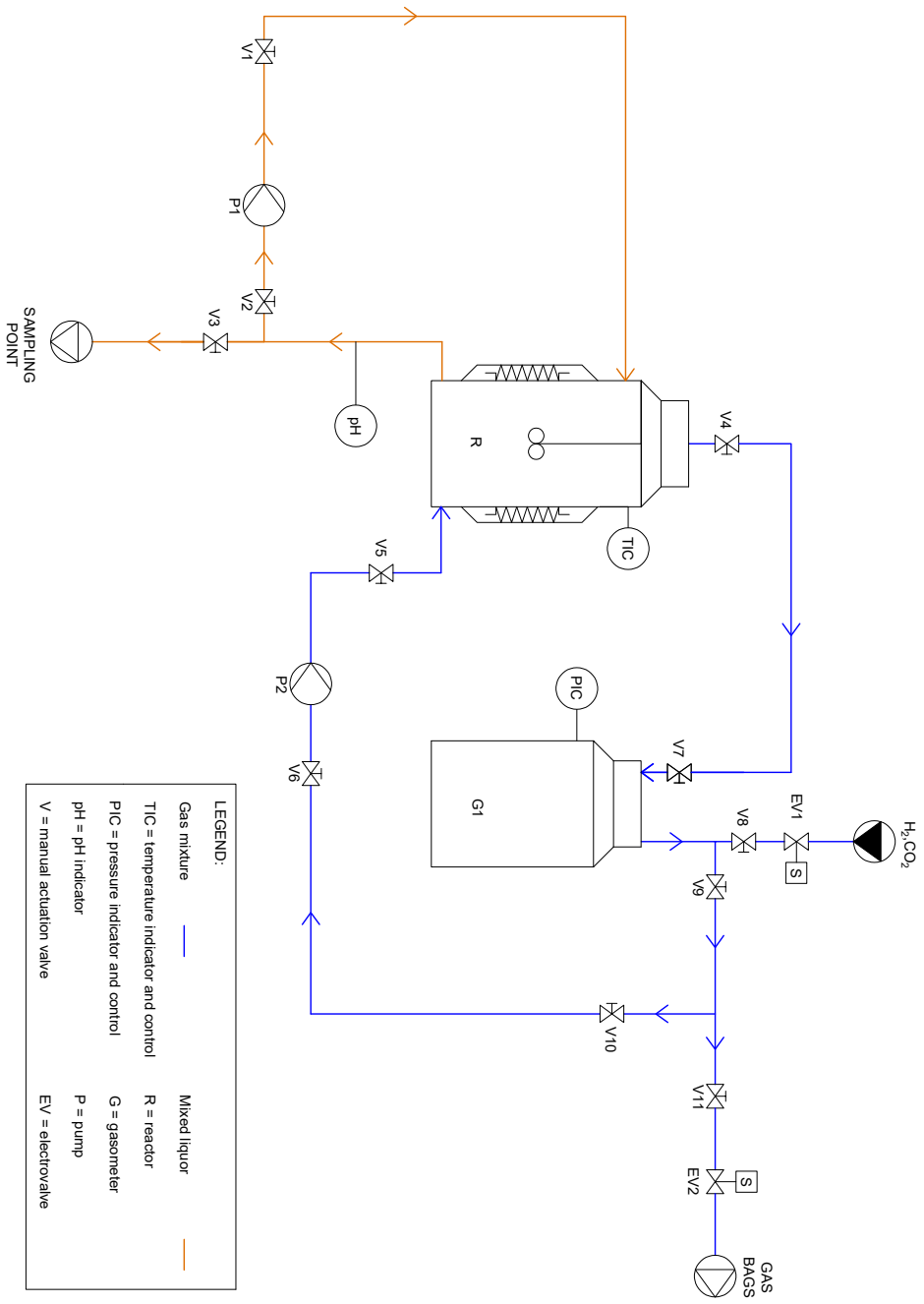

Figure 3.2: Configuration 1

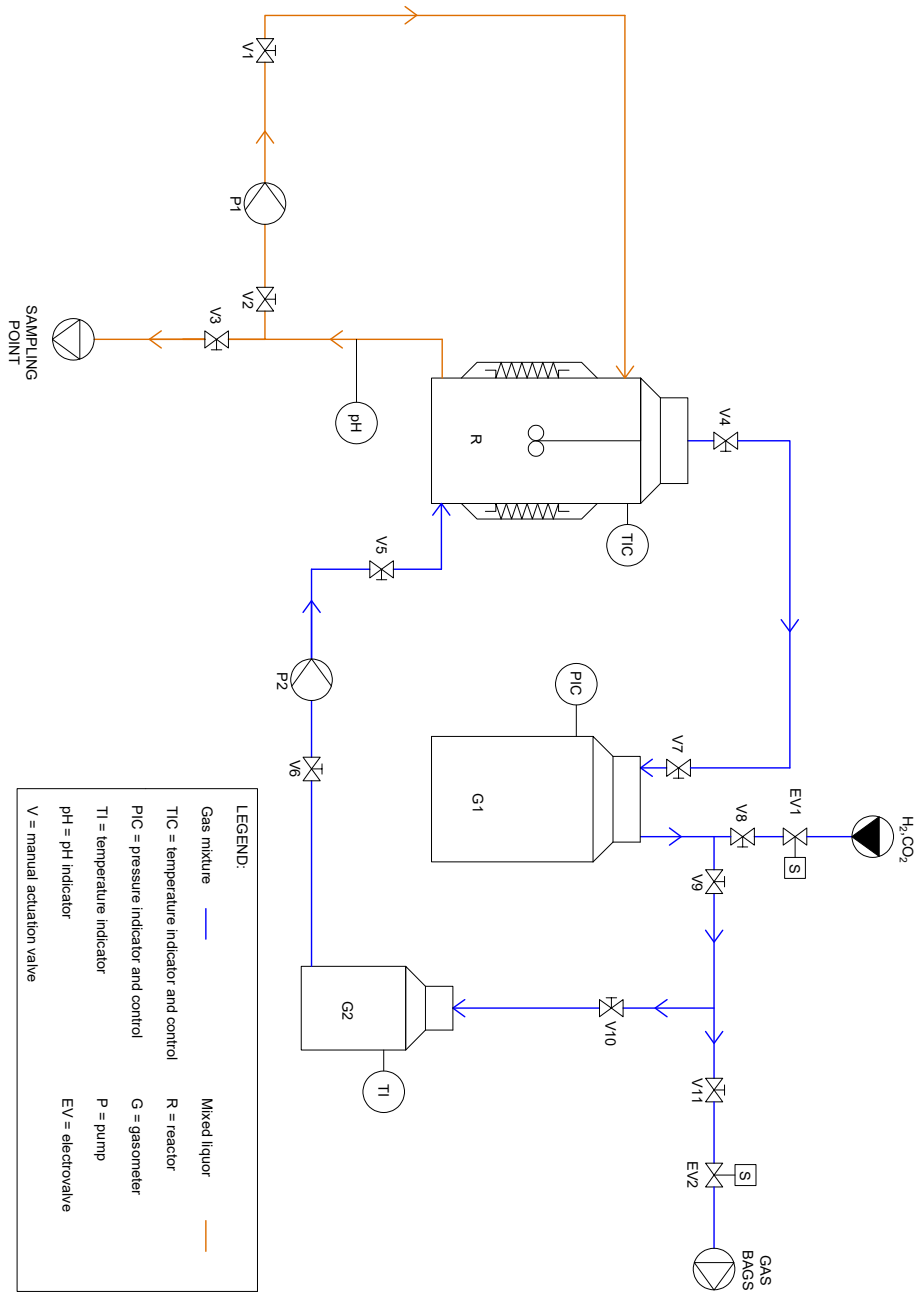

Figure 3.3: Configuration 2

closed, preventing further intake of the mixture. Considering the consumption of 5 moles in the gaseous phase (4 of H_2 and 1 of CO_2) during biomethanation, resulting in the production of a single mole of CH_4, a gradual decrease in pressure was observed. A discharge pressure of 1160 mbar was then set: upon reaching this value, measured by the PIC, the second electrovalve (EV2) was opened, allowing discharge to the specific polyvinyl fluoride (PVF) bags. In this way, the pressure continued to decrease until reaching a minimum of 1100 mbar, leading to the closure of EV2 and, simultaneously, the opening of EV1 to permit the re-entry of the mixture from the cylinder, thus restoring the pressure to its maximum value.
Through gas chromatography, the analysis of bags'content was conducted, evaluating the concentrations of H_2, CO_2, O_2, N_2, and CH_4 present within. Specifically, nitrogen concentration, and especially oxygen concentration, are expected to be low, as the process is intended to be anaerobic.
For the first two tests, the configuration depicted in Figure 3.2 was used; in the third test, to enhance data precision, a 0.3 L Schott bottle (G2) was introduced to accommodate a gas temperature indicator (TI), as observed in Figure 3.3. Additionally, in the third test, a pH control system was implemented, supplementing the measurements conducted in the preceding two trials: when the measured pH dropped below 6.8, the EV1 at the gas mixture inlet was closed, reopening only when the pH returned to higher values.
The measurement and control of various parameters (temperature, pressure, pH), as well as the opening of the electrovalves, are ensured by an Arduino system connected to a PC. The PC runs a continuous MATLAB script that regulates the operation of the process.

3.2 Results and discussion

Below are the results related to the three conducted tests. For each test, analyses were performed, and their methodologies are detailed in the appendix. To perform analyses related to biomass, a specific quantity of mixed liquor was extracted through the sampling point and an equal volume of digestate or tap water was reintroduced through the same point.

3.2.1 Test 1

The system was loaded with a quantity of digestate equal to 1.5 L, and both pumps operated continuously, ensuring the continuous recirculation of both the liquid and gaseous mixture. Following the startup, a daily biomass sampling of 100 mL was carried out, accompanied by the introduction of an equal volume of digestate.
From the analysis of the pressure trend in the system, as depicted in Figure 3.4, it is evident that the frequency of gas discharges into the bags gradually increases, suggesting a potential rise in the Methane Evolution Rate (MER). In Figure 3.5, indeed, an exponential increase in the daily average MER is observed, attributed to a rise in microorganisms. However, it is crucial to note that this MER value is considered theoretical, assuming that the entire pressure variation in the system is due to methane production.

Actually, the practical MER value obtained through GC analysis is markedly lower, at 0.0489 $\mathrm{L/L_{sludge}/d}$ in normal condition, indicating that the substrate is actively consumed but results in the production of acids in solution rather than methane. This implication is supported by both the pH trend, as shown in Figure 3.6, and the FOS-TAC trend, depicted in Figure 3.7: on the third day, the pH decreases dramatically, while the FOS (an indirect measure of volatile organic acids)

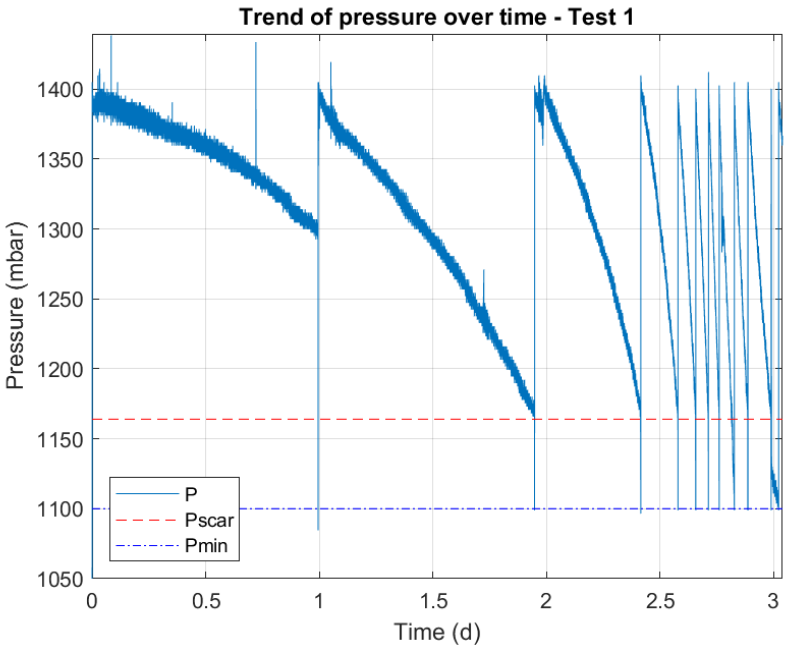

Figure 3.4: Trend of pressure over time for Test 1

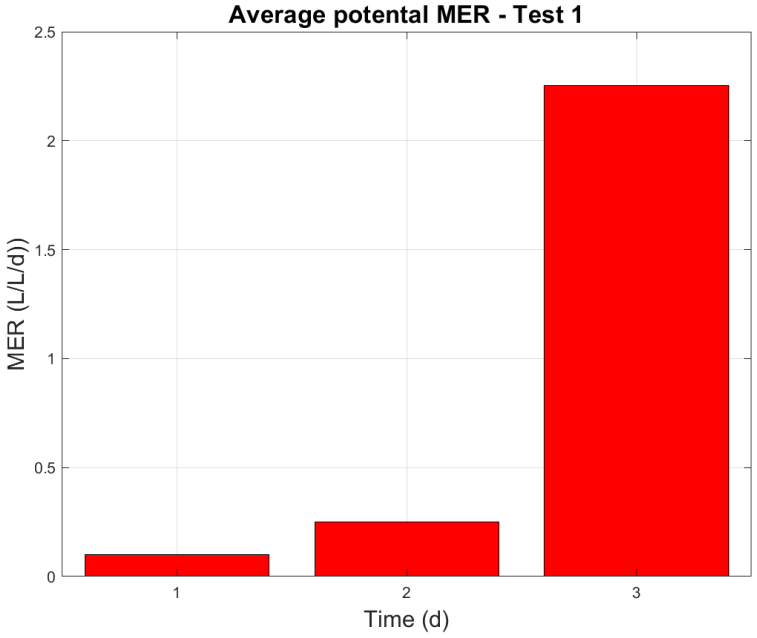

Figure 3.5: Trend of daily average potential MER over time for Test 1.

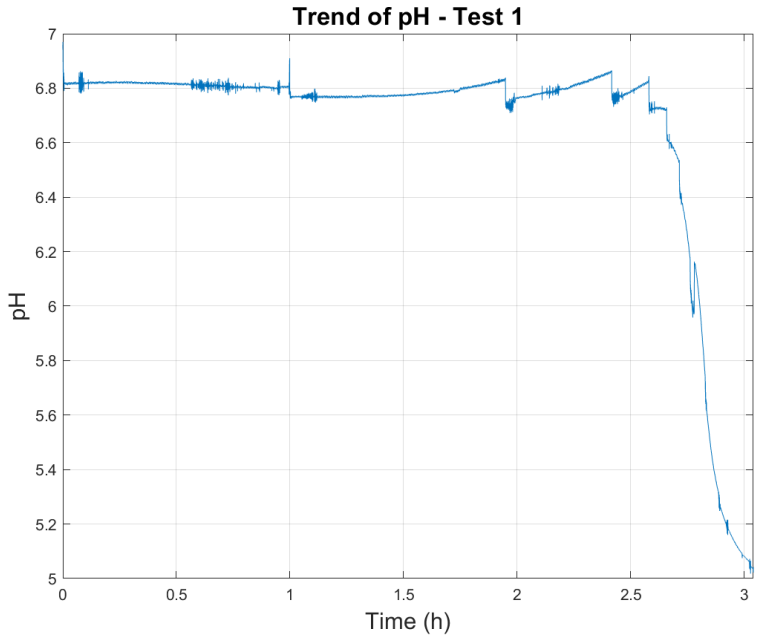

Figure 3.6: Trend of pH for Test 1

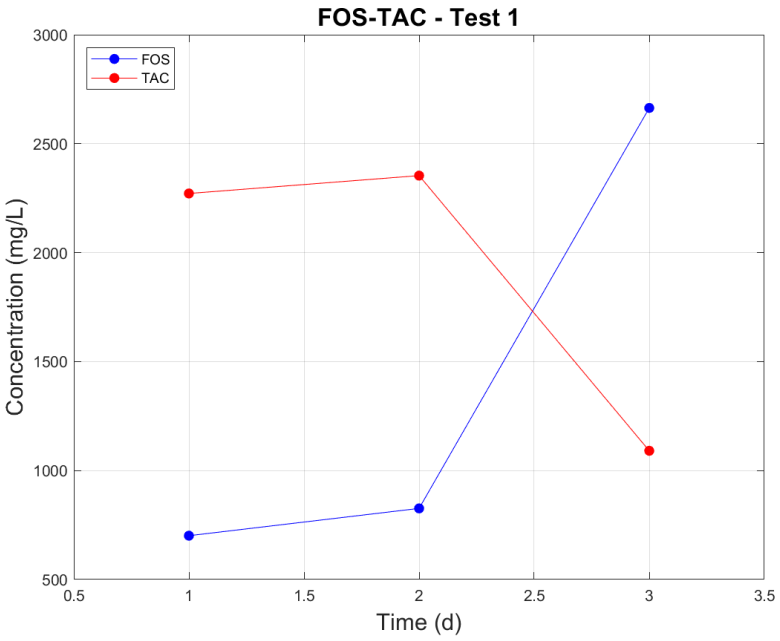

Figure 3.7: Trend of FOS-TAC for Test 1

increases significantly. As reported in the literature [11], hydrogenotrophic bacteria are known to be incapable of surviving under acidic pH conditions. Therefore, the test can be considered unsuccessful as it does not reflect the expected methane production. Therefore, the need arose to monitor the pH trend to ensure improved efficiency in methane production.

3.2.2 Test 2

The test was repeated under the same conditions as in Test 1. Analyzing the pressure trend, as shown in Figure 3.8, it can be observed that, similarly to the previous case, the frequency of discharges initially increases and then ceases entirely on the second day. Likewise, in Figure 3.9, it is evident that the daily average potential MER initially grows and then significantly decreases after the second day. The actual MER value recorded during these initial two days is $0.0134\,\mathrm{L/L_{sludge}/d}$ in normal conditions.

Observing the graph depicting pH and FOS-TAC trends, it is noticeable that on the second day, the pH tends to increase rapidly, and the TAC value (an indirect measure of alkalinity) remains relatively high. The test was deemed unsuccessful due to the depletion of gas within the cylinder. The absence of substrate input led to the inability of microorganisms to produce additional methane, resulting in a decrease in the partial pressure of carbon dioxide in the system. This, in turn, led to a reduction in dissolved CO_2 in the mixed liquor and, consequently, an increase in pH.

3.2.3 Test 3

With the second configuration, in Figure 3.3, the system was loaded with a quantity of digestate equal to 1.6 L. The liquid recirculation pump operated continuously,

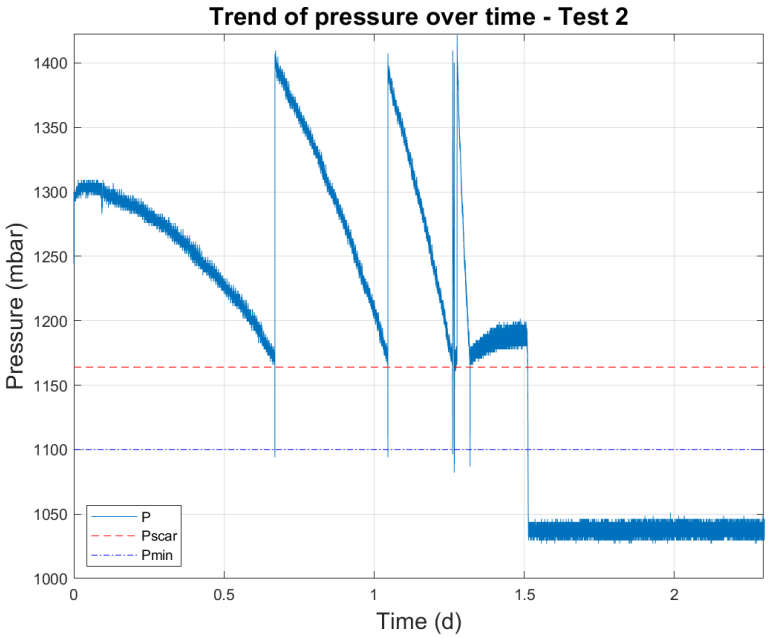

Figure 3.8: Trend of pressure over time for Test 2

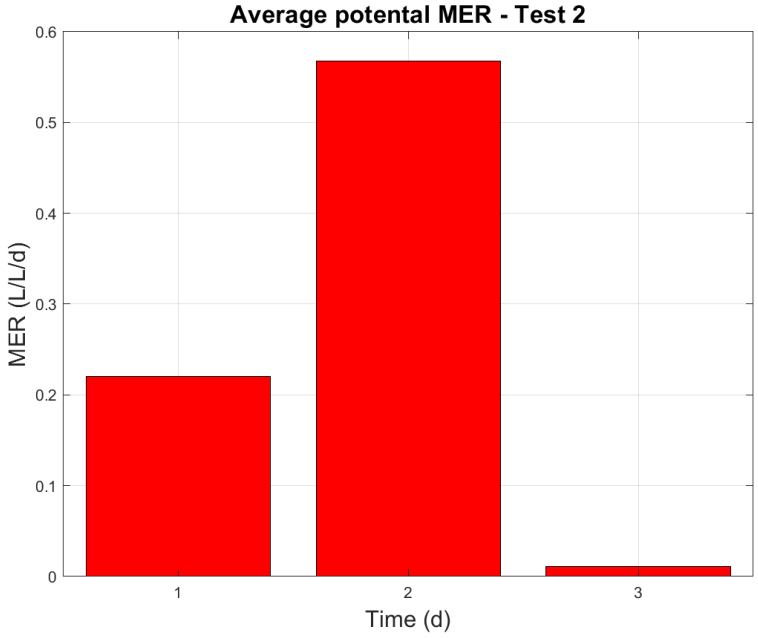

Figure 3.9: Trend of daily average potential MER over time for Test 2.

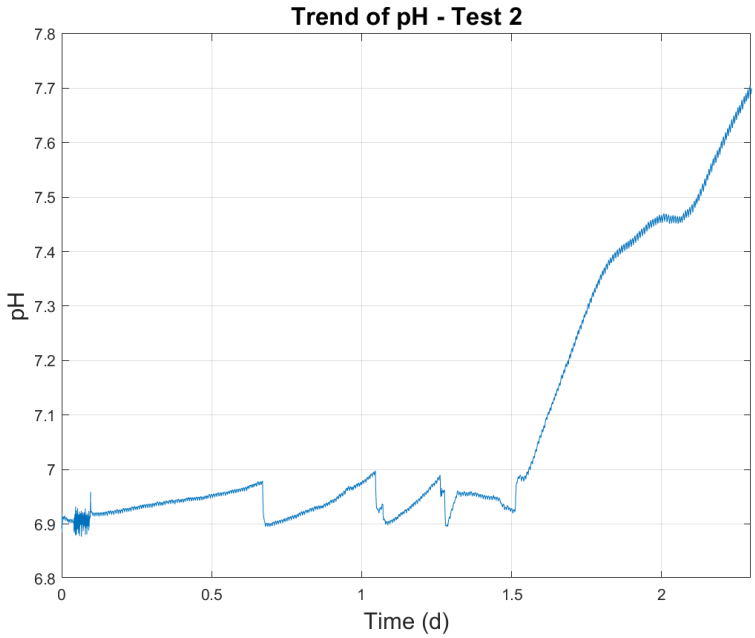

Figure 3.10: Trend of pH for Test 2

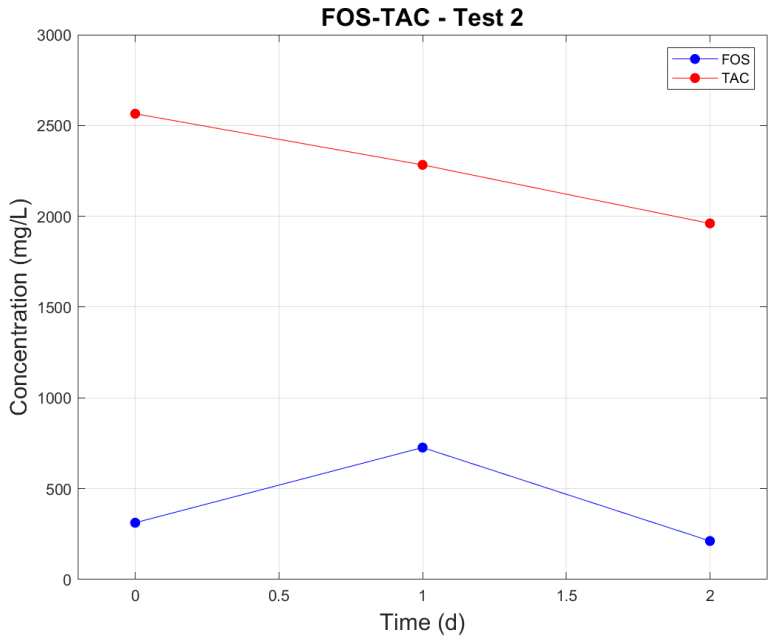

Figure 3.11: Trend of FOS-TAC for Test 2

while the gaseous recirculation pump operated by alternating 15 seconds of activity with 45 seconds of pause, in order to minimize the foam formation. Following the startup, daily biomass sampling was conducted from the system, maintaining a constant Hydraulic Retention Time (HRT) of 16 days, along with the introduction of an equal volume of tap water. It is important to note, as previously mentioned, that in this configuration, a pH control was implemented, regulating substrate input into the system.

Pressure, pH and MER trends

From the analysis of the pressure trend, as depicted in Figure 3.12, it is observed that the frequency of discharges gradually increases until the third day. On this day, as indicated in Figure 3.13, a significant decrease in pH below the established limit was noted. Consequently, there was a closure of the substrate input and a subsequent reduction in pressure. The situation returned to normal when, due to a lower partial pressure of CO_2, the pH again exceeded 6.8.

An important aspect to highlight is that, due to some errors in the Arduino control system, data related to the trends of pressure and pH for days 10, 11, 12 and 14 are not available.

The measured daily average MER values during different test days are reported in Figure 3.14, compared with the daily average values of potential MER calculated for each day. It is observed that potential MER and measured MER exhibit similar trends and values, indicating that the system is primarily progressing with methane production.

By the day 8, a significant decrease in MER is observed. This was caused by the occurrence of foam production in the reactor during system operation, which ended up in the gasometer. To recover the foam, the gasometer was emptied, resulting

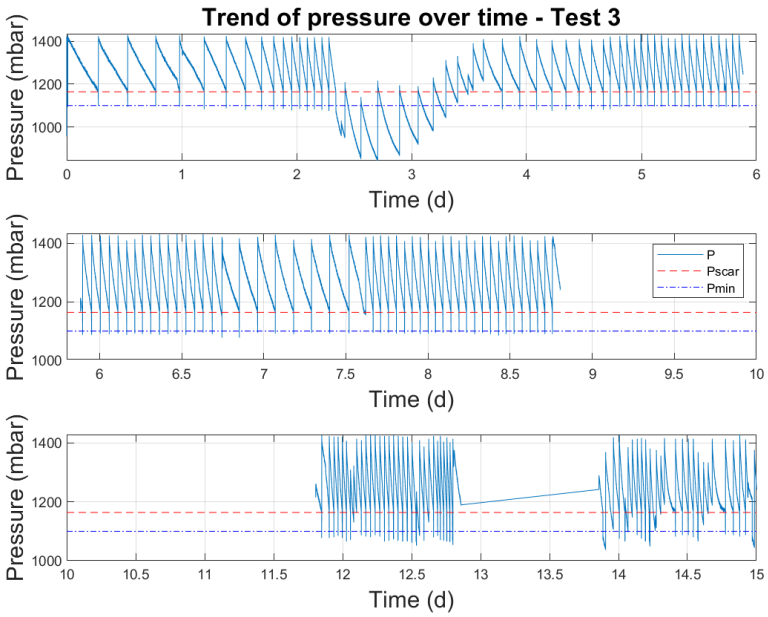

Figure 3.12: Trend of pressure over time for Test 3

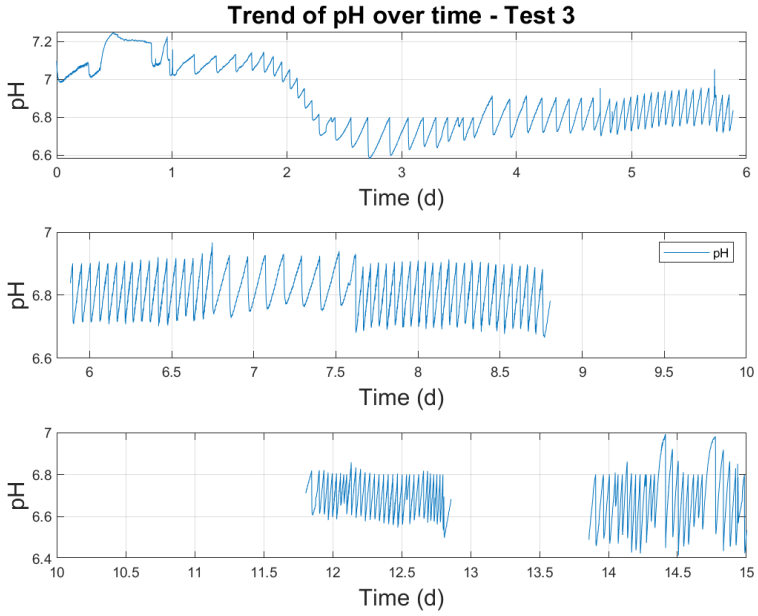

Figure 3.13: Trend of pH over time for Test 3

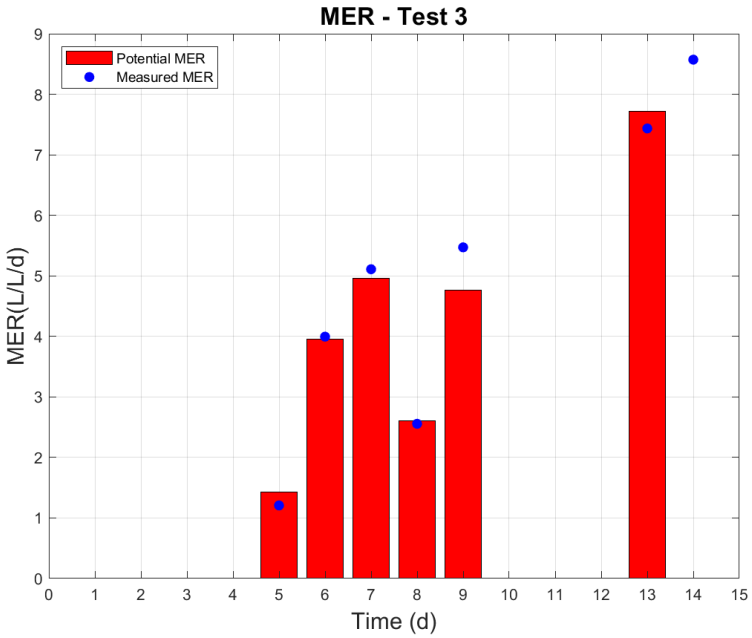

Figure 3.14: Trend of daily average of potential and measured MERs over time for Test 3

in a reduction in pressure, and consequently, a decrease in $\%CH_4$ concentration, along with additional substrate input into the reactor.

Volatile Fatty Acids

In Figure 3.16, the presence of volatile fatty acids (tVFAs) is analyzed, with acetic acid being the most prevalent. Initially, their concentration is minimal, but it reaches a value exceeding 2 g/L by day 5.

Subsequently, their values exhibit a decreasing trend. From the comparative analysis between the measured concentration values and the theoretical ones, obtained by considering the absence of biological processes but only the washout of the system due to the daily sampling, it emerges that the two parameters exhibit similar values and trends, as shown in Figure 3.15.

It is important to emphasize that, for the analysis of theoretical trends in the ab-

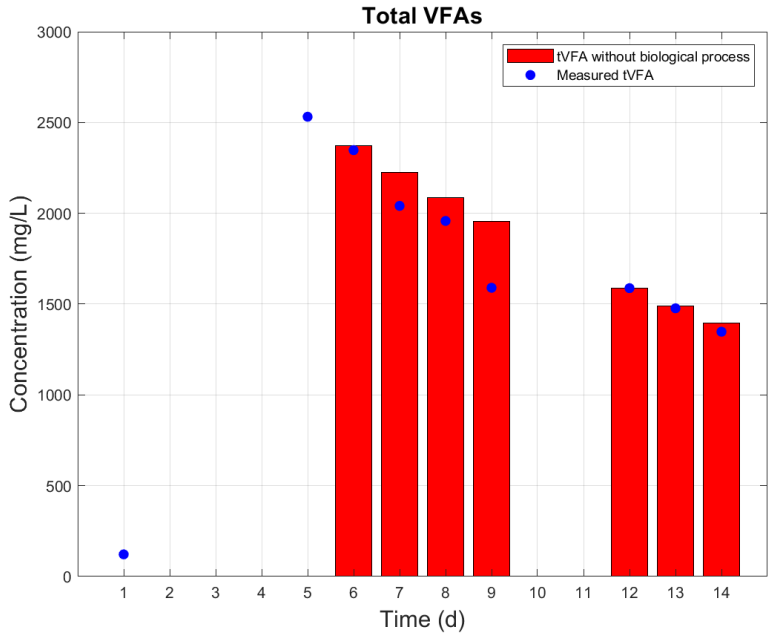

Figure 3.15: Trends of measured tVFAs concentrations and theoretical tVFAs concentrations without biological processes over time for Test 3.

sence of biological processes, the concentration measured by day 5 was considered as the initial concentration for the various parameters. This was done to ensure proper startup and complete homogeneity in concentrations during the initial days of reactor operation.

Figure 3.15 suggests that the presence of these volatile acids is not attributable to production from hydrogen, but rather is correlated with the biomass hydrolysis process.

The trend of the concentrations is thus expected to gradually decrease until reaching zero. Indeed, as observed in Figure 3.17, when analyzing a system with a HRT of 10 days and an initial concentration of 100%, with a gradual washout of the system, the concentration will reach 0% after a period of time equal to 3 times the HRT.

Therefore, for the analyzed system, considering the daily withdrawal of 100 mL

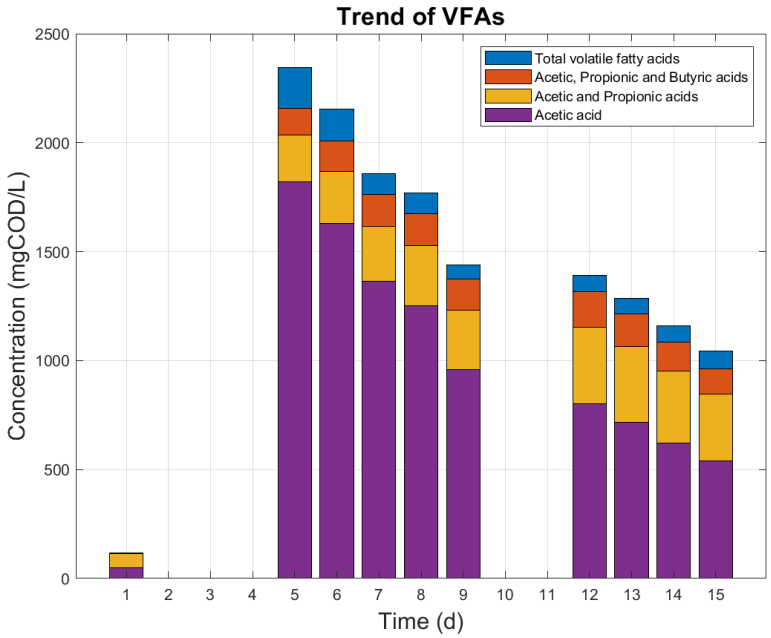

Figure 3.16: Trend of Volatile Fatty Acids (VFAs) concentrations, expressed in terms of COD, over time for Test 3.

of mixed liquor and the addition of an equal amount of tap water to maintain a constant working volume of 1.6 L, the HRT is 16 days. By 48 days, the system will have surpassed the period beyond which it will no longer be affected by the inoculum as it will have been completely washed out.

In the analysis depicted in Figure 3.18, it is evident that the mixed liquor, initially alkaline, already shows a significant increase in FOS by day 2, indicating an increase in volatile organic acids. This behavior is primarily attributed to the formation of VFAs through biomass hydrolysis. As seen in Figure 3.15, the measured values for FOS and TAC and their decreasing trend are also similar to those estimable in the absence of biological processes. This is mainly due to the washout of the reactor, with the input of tap water characterized by virtually negligible alkalinity and acidity.

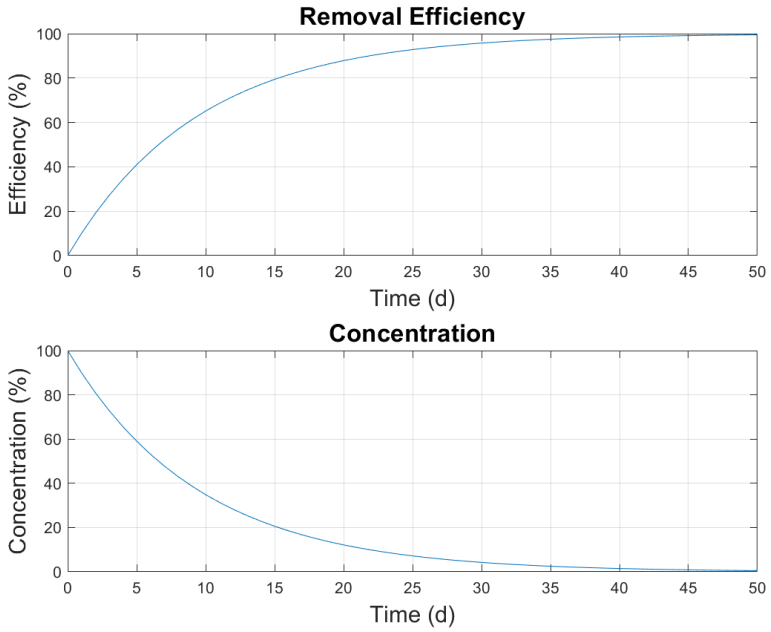

Figure 3.17: Effect of washout: after 3 times the HRT, concentrations reach zero.

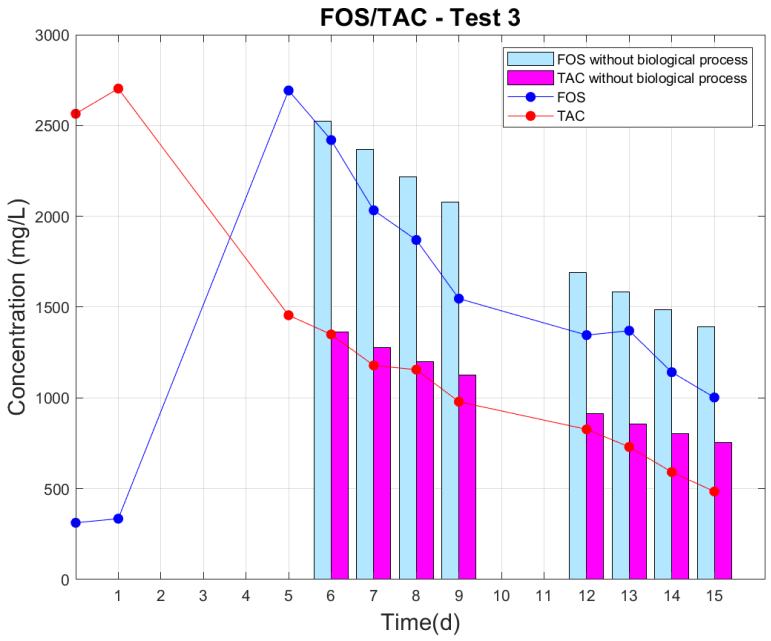

Figure 3.18: Trends of FOS-TAC over time for Test 3.

Macronutrients and biomass

Macronutrients are essential for the survival of microorganisms and for the development of the biomethanation process. Therefore, measurements of their concentrations were carried out, which showed a trend similar to that of the washout.
The concentrations of phosphorus and nitrogen are reported respectively in Figure 3.19 and Figure 3.20.
The measured trend is analogous to the theoretical one, in the absence of biological processes, except for a systematic error that remains almost constant on different days and may also be due to the analysis methods employed.

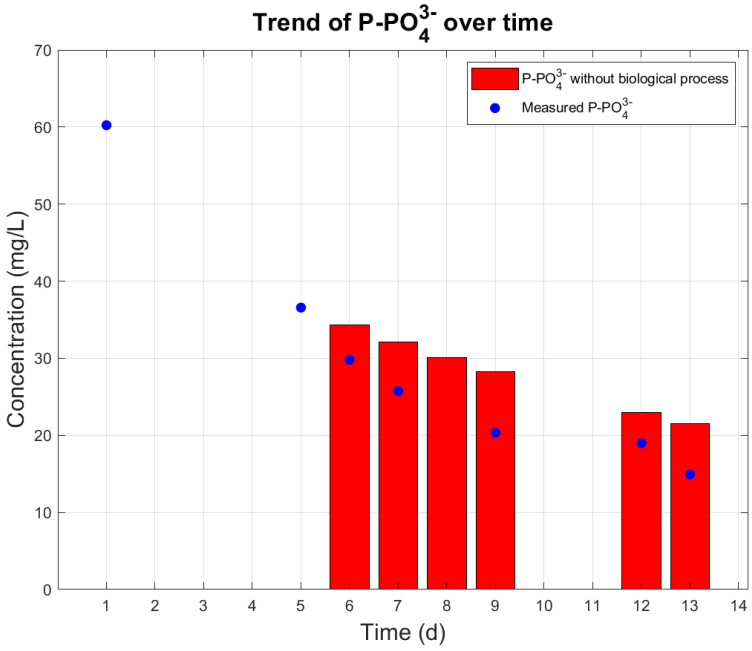

Figure 3.19: Trends of Orthophosphate - Phosphorous over time for Test 3.

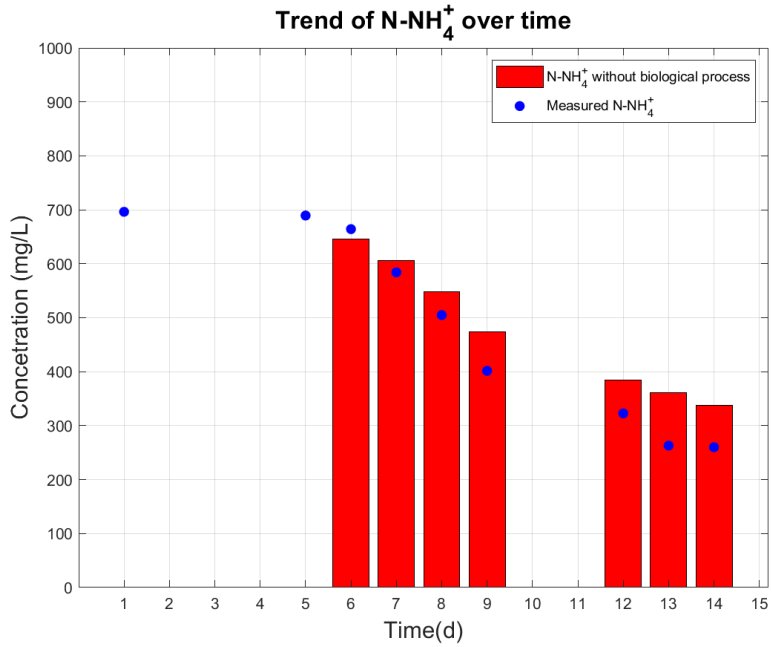

Figure 3.20: Trends of Ammoniacal Nitrogen over time for Test 3.

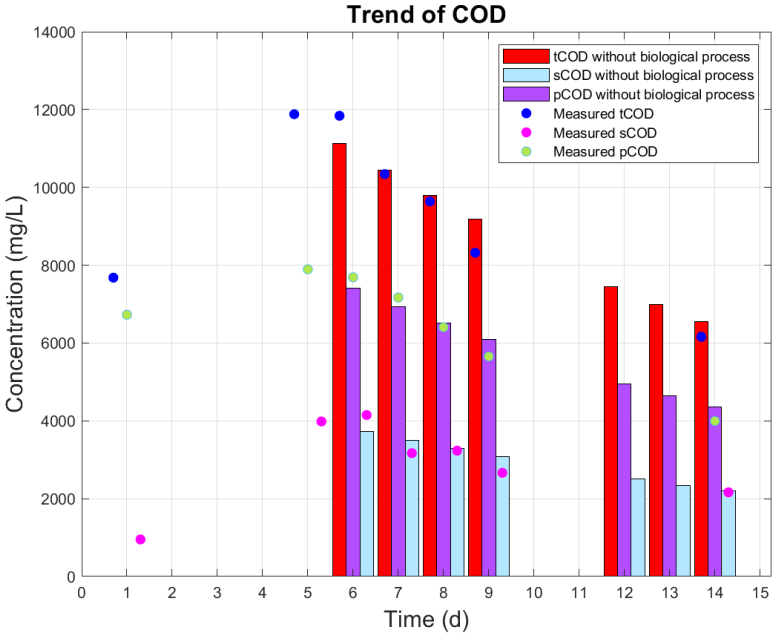

Figure 3.21: Trends of measured COD concentrations and its theoretical concentrations without biological processes over time for Test 3.

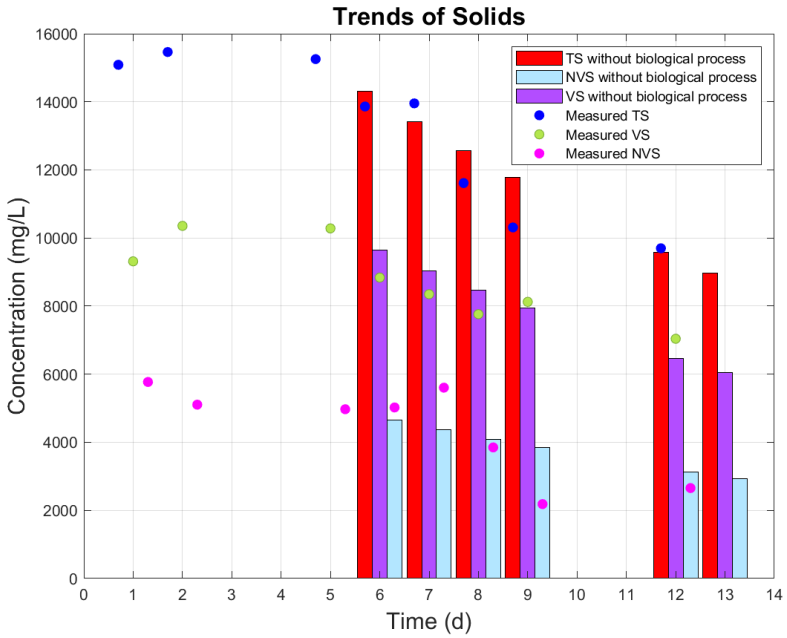

Figure 3.22: Trends of measured TS and NVS concentrations and their theoretical concentrations without biological processes over time for Test 3.

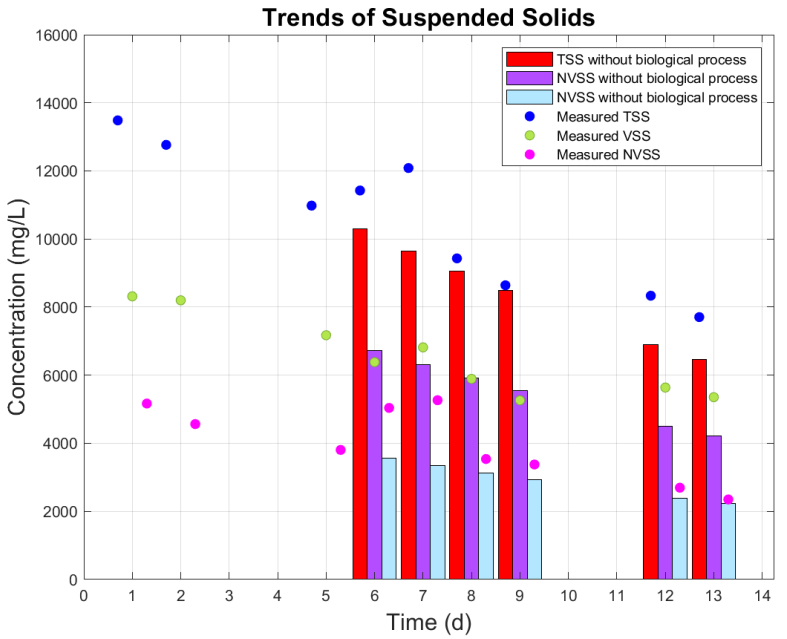

Figure 3.23: Trends of measured TSS and NVSS concentrations and their theoretical concentrations without biological processes over time for Test 3.

The analysis of COD and solids allows assessing the biomass trend within the system. Indeed, as evidenced in Figure 3.21, Figure 3.22 and Figure 3.23, the measured concentrations of particulate COD (pCOD), non-volatile solids (NVS), and non-volatile suspended solids (NVSS) exhibit a decreasing trend over time, indicating negative variations. This implies that the amount of biomass dying within the system is greater than the biomass produced daily. However, the trend deviates from the theoretical values expected in the absence of biological processes, indicating that, despite the washout, there is still some biomass production, consuming substrate.

Part III

Conclusion

Chapter 4

Conclusion

Hydrogen stands as a promising energy carrier, the utilization of which, if produced through entirely renewable sources, would render atmospheric CO_2 emissions negligible. However, it encounters various challenges, including storage, owing to its low energy density. Conversely, methane offers a more readily deployable alternative, benefitting from existing infrastructure for convenient storage and distribution. Biomethanation thus emerges as a viable option, leveraging green hydrogen as a feedstock, while also facilitating CO_2 recovery from other processes and limiting emissions.

The main objective of this work was to develop a laboratory-scale fed-batch and ex-situ biomethanation system under mesophilic conditions, ensuring high MER values. Additionally, the goal was to obtain results that could be extrapolated for the development of industrial-scale plants in various fields, including wastewater treatment.

4.1 Results interpretation

The tests have revealed several observations, detailed in the following paragraphs, which may be useful for the development of this technology, even on an industrial scale.

4.1.1 Methane Evolution Rate

The most evident observation concerns the MER values obtained during the various tests, which represent a crucial parameter for evaluating the efficiency of the analyzed systems.

Achieving high MER values indicates a system capable of producing large quantities of methane per unit of time, using smaller reactor volumes.

Particularly, in Test 1, it is observed how the uncontrolled operation of the system and the consequent development of an acidic environment lead to a very low effective MER (0.0489 $L/L_{sludge}/d$), significantly diverging from the potential production. This is due to the unfavorable reaction environment for the survival of hydrogenotrophic methanogenic microorganisms.

In Test 2 as well, a relatively low effective MER value (0.0134 $L/L_{sludge}/d$) is recorded, attributed to the absence of substrate due to the depletion of the H_2/CO_2 mixture inside the cylinder. This underscores the necessity of substrate as a raw material for the process to occur.

Test 3, on the other hand, exhibits more significant results, as depicted in Figure 3.14 and Table 4.2. By ensuring that the system operates under optimal pH conditions for the microorganisms, the system achieved elevated MER values, reaching 8.57 $L/L_{sludge}/d$ by day 14 and notably surpassing those reported in the literature such as Miehle et al. [26] with 2.21 $L/L_{sludge}/d$ under mesophilic conditions, and Voelklein et al. [38] with 3.7 $L/L_{sludge}/d$ under thermophilic conditions.

4.1.2 Apparent yield of microbial growth

To assess production, it is possible to determine the apparent yield of microbial growth Y using Equation 4.1, which provides information regarding the quantity of substrate used for biomass production. Here, ΔVSS represents the daily variation

in concentration of volatile suspended solids (mgVSS/L), while ΔH_2 represents the daily variation in hydrogen concentration, considered as substrate, expressed in terms of corresponding Chemical Oxygen Demand (mgCOD/L).

$$Y = \frac{\text{biomass produced}}{\text{consumed substrate}} = \frac{\Delta \text{VSS}}{\Delta H_2} \tag{4.1}$$

The estimation of Y may serve as a significant parameter for assessing system inefficiency. It provides insights into the amount of incoming substrate utilized for the production of additional biomass, rather than for the primary purpose of methane production within the reactor. Consequently, low values imply greater efficiency in the biomethanation process.

From Table 4.1, which reports the obtained values, it emerges that the results are consistent with literature values for anaerobic methanogenesis processes, typically falling within the range of 0.05 to 0.10 gVSS/gCOD [24]. However, an outlier value is observed by day 8, attributed, as mentioned in the previous chapter, to the excessive substrate input caused by the emptying of the gasometer. The results

Table 4.1: Values of biomass daily produced, substrate daily consumed and relative yields of microbial growth Y

Day	ΔVSS (mgVSS/L)	ΔH_2 (mgCOD/L)	Y (gVSS/gCOD)
6	116.67	3447.31	0.03
7	1025.00	7961.01	0.13
8	790.00	3180.22	0.25
9	433.33	7289.97	0.06
12	926.67	8323.10	0.11
13	628.33	5608.10	0.11

obtained from the estimation demonstrate an optimal efficiency of the system in terms of substrate consumption. Further, more certain confirmation could be obtained by assessing the effective yield of microbial growth through measurements.

4.1.3 Control of pH

An aspect that emerged from Test 1 concerns the pH values. The system, operating autonomously, tends over time to create excessively acidic environments.
As reported in the literature and confirmed during the test, this leads to the death of hydrogenotrophic microorganisms and hinders methane production, which, indeed, represents the main objective in the biomethanation process.
It is therefore advisable to work under pH conditions not lower than 6.8.
An alternative could be to work with higher H_2/CO_2 ratios compared to the stoichiometric ones employed. With a lower partial pressure of carbon dioxide in the reactor, the amount dissolved in the mixed liquor is reduced, resulting in a higher pH. This approach would also result in an increase in the Low Heating Value of the resulting gas since the contribution associated with CO_2 is zero, as it is already fully oxidized.

4.1.4 Methane and hydrogen contents

As described in the previous chapter, in Test 3, MER values exceeding 8 $L/L_{sludge}/d$ are recorded, significantly higher compared to the values reported in literature such as Miehle et al. [26] and Voelklein et al. [38]. Nevertheless, these lower values are compensated by a higher methane content observed, respectively, at 99% and 96%.

In Figure 4.1, the concentration values of the different components measured in the gas mixture are reported. It is observed that the methane content increases over time, reaching 89% on the last day. However, it is accompanied by a hydrogen content of 8%. This concentration is not negligible and significantly exceeds the H_2 limit value for the introduction of the mixture into the natural gas transportation and distribution grid, set at 0.5 %mol in the technical report UNI/TR 11537.[15]

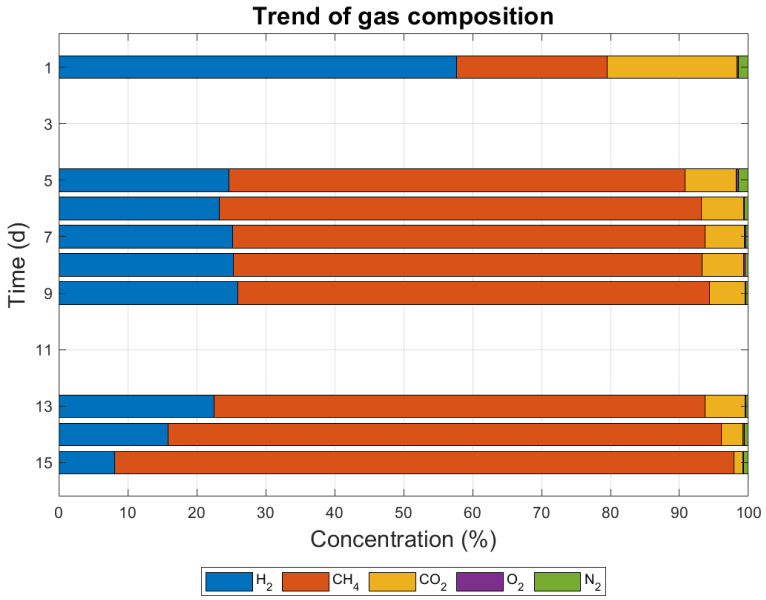

Figure 4.1: Trend of gas composition for Test 3

An approach to optimize the system could involve reducing the partial pressure of hydrogen and carbon dioxide within the system. This adjustment may result in a decrease in the MER achieved by the system under equivalent conditions. Nevertheless, it would allow for the production of a mixture that complies with the limit value and could be directly injected into the grid.

4.1.5 Macronutrients

Another aspect to consider is represented by the concentrations of nitrogen and phosphorus in the reactor, two macronutrients necessary for the survival of microorganisms. As observed in the previous chapter, because of the system washout, their concentrations gradually decrease day by day.

Indeed, as observed in Figure 3.17, their are expected to reach a value of zero after a time interval equal to three times the Hydraulic Retention Time. Therefore,

it may become crucial, in relation to the quantity of microorganisms present, to proceed with the addition of salts into the system to ensure that concentration values remain constant.

The *BTMI* (Market Regulation, Development, and Transparency Company for the dissemination of prices and economic information, established by the Minister of Agricultural and Forestry Policies in 2006) emphasizes that, with the ongoing conflict between Russia and Ukraine, fertilizer prices have increased significantly, reaching values even more than double compared to previous years (675 euros/ton for ammonium nitrate and 678 euros/ton for ammonium triple phosphate).[3]

This expenditure should then be accounted for among the operational costs of the system on industrial scale and it is not negligible.

4.1.6 Heat production

Given the considerations outlined in Paragraph 2.5.8, heat production constitutes a crucial aspect warranting careful analysis, as it can promote the implementation of the biomethanation process across various scopes.

Taking into account the results from Test 3, it was possible to assess whether the system is *thermal self-sufficient*, that is, if it is able to maintain thermal equilibrium without relying on external sources. Consequently, the daily intake of 100 mL of water at a temperature of 15°C into the reactor was considered. Utilizing Equation 4.2, the amount of heat necessary to elevate this volume to the system's temperature of 38°C was estimated. In this formula, E_{th} represents the required heat (kJ); $m_{\mathrm{H_2O}}$ represents the input water mass (g); C_p is the specific heat of water, equal to 4.186 J/g/°C; T_{system} and T_i represent the system temperature (°C) and the water inlet temperature (°C) respectively.

$$E_{th} = m_{\mathrm{H_2O}} \cdot C_p \cdot (T_{\mathrm{system}} - T_i) \tag{4.2}$$

The daily required heat, therefore, amounts to 9.63 kJ. Taking into account the

Table 4.2: Values of the produced MER, the corresponding available heat, the daily required heat and the remaining excess heat after the input of 100 mL of water.

MER (**L/L$_{\text{sludge}}$/d**)	**Available Heat (kJ)**	**Required Heat (kJ)**	**Excess Heat (kJ)**
1.21	14.22	9.63	4.59
4.00	47.06	9.63	37.43
5.11	60.18	9.63	50.55
2.56	30.11	9.63	20.48
5.47	64.44	9.63	54.81
7.44	87.57	9.63	77.94
8.57	100.96	9.63	91.33

reaction occurring during the biomethanation process (Equation 1.4) and its enthalpy variation ΔH_r equal to -165 kJ/mol, it is possible to determine the amount of energy available $E_{\text{th available}}$ (kJ) from the produced MER using Equation 4.3.

$$E_{\text{th available}} = \frac{\text{MER}}{V_{\text{mol}}} \cdot V_{\text{mixed liquor}} \cdot \Delta H_r \tag{4.3}$$

Here, MER indicates the measured *Methane Evolution Rate* (L/L$_{\text{sludge}}$/d), V_{mol} is the molar volume in normal conditions, equal to 22.414 L/mol; $V_{\text{mixed liquor}}$ is the volume of the mixed liquor into the reactor (L), while ΔH_r represents the enthalpy variation of the biomethanation reaction (kJ/mol).

The availability of energy can therefore be assessed to determine if it consistently exceeds the amount required to heat the incoming water. From the analysis of their values, as reported in Table 4.2, it can be observed that the system can be deemed thermally self-sufficient. The heat generated from the reaction allows maintaining the system temperature at 38°C without the need for external heat sources. However, it is important to emphasize the need to limit heat production to

avoid excessively high temperatures and consider the implementation of a cooling system.

4.2 Conclusion remarks

The production of methane from hydrogen is particularly advantageous for several reasons, among which emerges the ease of its transportation and its higher heating value if used as a fuel. For the development of biomethanation technology, even on an industrial scale, it is necessary to take into account the aspects highlighted in the previous paragraph and summarized below.

- It is necessary to introduce pH control systems to ensure the survival of hydrogenotrophic methanogenic microorganisms and promote the increase of MER values. An alternative could also be to work with higher H_2/CO_2 ratios.
- It is important to ensure a sufficient MER value, accompanied by a high methane content and a minimal hydrogen content, below the limit of 0.5 mol%[15]. To achieve this, it may be advantageous to operate under lower partial pressure conditions of H_2 and CO_2.
- The daily washout of the system results in a significant decrease in the concentration of various substances over time, including macronutrients. To ensure the survival of microorganisms, it is necessary to introduce appropriate salts, the costs of which are high.
- The system is thermally self-sufficient. The exothermic nature of the process can therefore serve as a useful energy source, capable of balancing the costs of nitrogen and phosphorus salts. Furthermore, to maximize heat production, it could be a valid option to increase the MER production by operating at higher working pressures (up to 10 bar) and/or under thermophilic conditions

(55°C) or hyperthermophilic conditions (78°C). The produced heat must be controlled and this allows the reactor to be implemented in specific contexts, such as wastewater treatment plants (WWTPs). In particular, heat can be channeled through appropriate heat exchangers and used in other processes, such as:

- *Anaerobic Digestion of sludge*, upstream of the biomethanation process, which provides the CO_2 used as a raw material for the process;
- *Thermal Drying of sludge*, during which heat is supplied to the produced sludge to remove moisture, reduce volume, and facilitate transport and disposal.

Part IV

Appendices

Appendix A

Methodical analyses

A.1 Determination of Total and Volatile Solids

1. Weigh three crucibles (taken from the oven at 105 °C and allowed to cool in a desiccator for about 15 minutes) using a four-decimal-place balance (**crucible**).
2. Prepare three samples of sludge (not centrifuged and not filtered) in two crucibles and weigh them (**crucible + sample**).
3. Place the samples in an oven at 105 °C for at least 12 hours.
4. Weigh the samples (**crucible + total solids (105°C)**).
5. Place the samples in a muffle furnace at 600 °C for at least 2 hours (noting on a sheet the order of the crucibles, as the ink gets removed).
6. Weigh the samples (**crucible + non-volatile solids (600°C)**).

A.2 Determination of Total and Volatile Suspended Solids

1. Weigh 2 glass slides (**glass**);
2. Weigh the glass slides with filters (**glass + filter**);

3. Conduct vacuum filtration using **3 mL of non-centrifuged sludge** drawn with a specific pipette.
4. Place the used filter on the respective glass slide and in an oven at 105°C for at least 12 hours.
5. Weigh the samples (**glass + filter + total suspended solids (105°C)**);
6. Weigh 2 empty crucibles (**empty crucible**);
7. Place the samples in the crucibles;
8. Place the samples in a muffle furnace at 600 °C for at least 2 hours (noting the order of the crucibles);
9. Weigh the samples (**crucible + ashes (600°C)**).

A.3 Determination of FOS and TAC

Titrate with H2SO4 on the sample under agitation to reach pH 5 and pH 4.4. The sample consists of: **20 mL of non-centrifuged sample + 20 mL of distilled H2O**. Record the values of FOS, TAC, their ratio, and the pH.

A.4 Centrifugation and Filtration

A sample should be centrifuged for 15 minutes at 10000 rpm. Then filter it using 0.45 µm filters.

A.5 Measurement of NH_4^+ Concentration

The Spectroquant® Ammonium Test method is employed, enabling work within the concentration range of 0.010 to 3 mg/L NH_4-N. It involves three reagents, denoted as R1, R2, and R3.

1. Prepare a cuvette containing 5 mL of the filtered sample to be analyzed.
2. Add 0.60 mL of R1 and mix.
3. Add a level microspoonful of R2 and vigorously agitate until the reagent is completely dissolved.
4. Allow to stand for 5 minutes.
5. Add 4 drops of R2 and mix.
6. Let stand for 5 minutes.
7. Prepare a cuvette containing the blank in the same manner, using 5 mL of distilled water.

Readings are taken using a spectrophotometer at a wavelength of 690 nm. Dilution factors are applied as necessary during the testing process.

A.6 Measurement of P-PO_4^{3-} Concentration

The Nanocolor® orthophosphate method is utilized for the measurement, facilitating analysis within a concentration range of 0.2 to 6.6 mg/L PO_4-P. This method involves two reagents, denoted as R1 and R2.

1. In a 25 mL flask, 20 mL of the sample to be analyzed is added.
2. 1 mL of R1 is added and mixed.
3. 1 mL of R2 is added and mixed.
4. The volume is brought to 25 mL by adding distilled water.
5. Allow to stand for 10 minutes.

6. Similarly, prepare a flask containing the blank, using 20 mL of distilled water in place of the sample.

The readings are taken using a spectrophotometer at a wavelength of 436 nm. Dilution factors are applied as necessary during the testing process.

A.7 Determination of VFAs Concentration

VFAs concentrations of the raw sludge and biological treated samples were analyzed using a gas chromatography (GC) Shimadzu GC 2010 Pro equipped with a split injector and flame ionization detection (FID) system.

A.8 Determination of Total and Soluble Chemical Oxygen Demand

The COD concentration was determined by photometric detection employing a linear relationship between absorbance and concentration (Lovibond® Water Testing Tintometer® Group kits).

Glossary

Abbreviations

PtL	Power-to-Liquid
PtG	Power-to-Gas
PtF	Power-to-Fuel
PtM	Power-to-Methane
CSTR	Continuous-Stirred Tank Reactor
TBR	Trickle Bed Reactor
PFR	Plug-flow Reactor
RFNO	Renewable Fuels of Non-Biological Origins
AEC	Alkaline Electrolyzer
PEM	Polymer electrolyte membrane
SOE	Solid Oxide Electrolyzer
HAC	Homoacetogens
SAO	Syntrophic acetate oxidizers
AM	Acetoclastic methanogens
HM	Hydrogenotrophic methanogens
WWTP	Wastewater Treatment Plant
GC	Gas chromatography

Chemical compounds

CH_4	Methane
CO	Carbon monoxide
CO_2	Carbon dioxide
H_2	Hydrogen
N_2	Nitrogen
H_2O	Water
NH_3	Ammonia
CH_3COOH	Acetic acid
$N-NH_4^+$	Ammoniacal Nitrogen
$P-PO_4^{3-}$	Orthophosphate Phosphorous

Parameters

MER	Methane Evolution Rate
VFA	Volatile Fatty Acids
COD	Chemical Oxygen Demand
pCOD	Particolate COD
sCOD	Soluble COD
tCOD	Total COD
TS	Total Solids
VS	Volatile Solids
NVS	Non-volatile solids
TSS	Total suspended solids
VSS	Volatile suspended solids
NVSS	Non-volatile suspended solids
HRT	Hydraulic Retention Time
ΔH_r	Enthalpy variation of reaction
$\Delta G'^{\circ}$	Standard Gibb's free energy
H_{2g}	H_2 concentration in gas phase
H_{2l}	H_2 concentration dissolved in the liquid phase
R_t	Rate of substrate utilization by biomass
$k_L\alpha$	Gas-liquid mass transfer coefficient
L_R	Liters of reactor
L_{sludge}	Liters of sludge
T	Temperature
P	Pressure
Pw	Power
V	Volume
V_{mol}	Molar volume
E_{th}	Heat
Q	Flow rate
Cp	Specific heat
m	Mass
Y	Yield of microbial growth
ΔH_2	Daily variation of H_2 concentration
ΔVSS	Daily variation of VSS concentration
C	Concentration
δ	Thickness

Bibliography

[1] Irini Angelidaki, Laura Treu, Panagiotis Tsapekos, Gang Luo, Stefano Campanaro, Henrik Wenzel, and Panagiotis G Kougias. Biogas upgrading and utilization: Current status and perspectives. *Biotechnology advances*, 36(2): 452–466, 2018.

[2] Ilaria Bassani, Panagiotis G Kougias, Laura Treu, Hugo Porté, Stefano Campanaro, and Irini Angelidaki. Optimization of hydrogen dispersion in thermophilic up-flow reactors for ex situ biogas upgrading. *Bioresource technology*, 234:310–319, 2017.

[3] BTMI Scap. The dynamics of wholesale fertilizer prices, 2022. URL `https://www.bmti.it/wp-content/uploads/2022/03/BMTI-scheda-fertilizzanti-mar-22-1.pdf`.

[4] VIOLA CORBELLINI. Biological h2-mediated in-situ biogas upgrading. 2019.

[5] Nicolaas Engelbrecht, Mads U Sieborg, Lars DM Ottosen, and Michael VW Kofoed. Metabolic heat production impacts industrial upscaling of ex situ biomethanation trickle-bed reactors. *Energy Conversion and Management*, 299:117769, 2024.

[6] European Union. Directive 2009/28/ec, 2009. URL `https://eur-lex.europa.eu/legal-content/EN/TXT/PDF/?uri=CELEX:32009L0028&from=SK`.

[7] European Union. Renewable energy directive ii, directive eu/2018/2001,

2018. URL https://eur-lex.europa.eu/legal-content/EN/TXT/PDF/?uri=CELEX:32018L2001.

[8] European Union. Renewable energy directive iii, directive eu/2023/2413, 2023. URL https://eur-lex.europa.eu/legal-content/EN/TXT/PDF/?uri=OJ:L_202302413.

[9] Eurostat. Net electricity generation by type of fuel - monthly data, 2022. URL https://ec.europa.eu/eurostat/databrowser/view/NRG_CB_PEM__custom_5180368/default/table?lang=en.

[10] Lipei Fu, Zhangkun Ren, Wenzhe Si, Qianli Ma, Weiqiu Huang, Kaili Liao, Zhoulan Huang, Yu Wang, Junhua Li, and Peng Xu. Research progress on co2 capture and utilization technology. *Journal of CO2 Utilization*, 66:102260, 2022.

[11] Jean-Louis Garcia, Bharat KC Patel, and Bernard Ollivier. Taxonomic, phylogenetic, and ecological diversity of methanogenic archaea. *Anaerobe*, 6(4): 205–226, 2000.

[12] Karim Ghaib and Fatima-Zahrae Ben-Fares. Power-to-methane: A state-of-the-art review. *Renewable and Sustainable Energy Reviews*, 81:433–446, 2018.

[13] A Giuliano, CM Cellamare, L Chiarini, S Tabacchioni, and L Petta. Evaluation of the controlled hydrodynamic cavitation as gas mass transfer system for ex-situ biological hydrogen methanation. *Chemical Engineering Journal*, 471:144475, 2023.

[14] Maria Grahn, Selma Brynolf, Maria Taljegård, and Julia Hansson. Electrofuels: a review of pathways and production costs. In *Conference Proccedings TMF-Aachen*, 2016.

[15] Italian Regulatory Authority for Energy, Networks and Environment (ARERA). Update of connection directives of biomethane production plants to the networks of natural gas and implementation of the provisions of decree 2 march 2018, 2018. URL `https://www.arera.it/fileadmin/allegati/docs/18/361-18.pdf`.

[16] Brian Dahl Jønson, Panagiotis Tsapekos, Muhammed Tahir Ashraf, Martin Jeppesen, Jens Ejbye Schmidt, and Juan-Rodrigo Bastidas-Oyanedel. Pilot-scale study of biomethanation in biological trickle bed reactors converting impure co2 from a full-scale biogas plant. *Bioresource Technology*, 365:128160, 2022.

[17] PG Kougias, Panagiotis Tsapekos, L Treu, M Kostoula, S Campanaro, G Lyberatos, and Irini Angelidaki. Biological co2 fixation in up-flow reactors via exogenous h2 addition. *Journal of Biotechnology*, 319:1–7, 2020.

[18] Melike Kozak, Emre Oğuz Köroğlu, Kevser Cirik, and Zeynep Zaimoğlu. Evaluation of ex-situ hydrogen biomethanation at mesophilic and thermophilic temperatures. *International Journal of Hydrogen Energy*, 47(34):15434–15441, 2022.

[19] L Laguillaumie, M Peyre-Lavigne, A Grimalt-Alemany, HN Gavala, IV Skiadas, E Paul, and C Dumas. Controlling the microbial competition between hydrogenotrophic methanogens and homoacetogens using mass transfer and thermodynamic constraints. *Journal of Cleaner Production*, 414:137549, 2023.

[20] Lardon, Laurent. Biocat-power to gas technology by biological methanation, 2017. URL `https://www.electrochaea.com/wp-content/uploads/2018/03/201803_Data-Sheet_BioCat-Plant.pdf`.

[21] Zhihao Liu, Xinhua Gao, Bo Liu, Qingxiang Ma, Tian-sheng Zhao, and Jianli

Zhang. Recent advances in thermal catalytic co2 methanation on hydrotalcite-derived catalysts. *Fuel*, 321:124115, 2022.

[22] Zhihao Liu, Xinhua Gao, Kangzhou Wang, Jie Liang, Yongjun Jiang, Qingxiang Ma, Tian-Sheng Zhao, and Jianli Zhang. A short overview of power-to-methane: Coupling preparation of feed gas with co2 methanation. *Chemical Engineering Science*, 274:118692, 2023.

[23] JP Megonigal, ME Hines, and PT Visscher. 10.8—anaerobic metabolism: Linkages to trace gases and aerobic processes. *Treatise on Geochemistry, 2nd ed.; Holland, HD, Turekian, KK, Eds*, pages 273–359, 2014.

[24] Leonard Metcalf, Harrison P Eddy, and Georg Tchobanoglous. *Wastewater engineering: treatment, disposal, and reuse*, volume 4. McGraw-Hill New York, 1991.

[25] Frédéric D Meylan, Vincent Moreau, and Suren Erkman. Material constraints related to storage of future european renewable electricity surpluses with co2 methanation. *Energy Policy*, 94:366–376, 2016.

[26] Maximilian Miehle, Max Hackbarth, Johannes Gescher, Harald Horn, and Andrea Hille-Reichel. Biological biogas upgrading in a membrane biofilm reactor with and without organic carbon source. *Bioresource technology*, 335: 125287, 2021.

[27] Jarosław Milewski, Janusz Zdeb, Arkadiusz Szczęśniak, Aliaksandr Martsinchyk, Jakub Kupecki, and Olaf Dybiński. Concept of a solid oxide electrolysis-molten carbonate fuel cell hybrid system to support a power-to-gas installation. *Energy Conversion and Management*, 276:116582, 2023.

[28] Amira Nemmour, Abrar Inayat, Isam Janajreh, and Chaouki Ghenai. Green hydrogen-based e-fuels (e-methane, e-methanol, e-ammonia) to support clean

energy transition: A literature review. *International Journal of Hydrogen Energy*, 2023.

[29] Norafneeza Norazahar, Faisal Khan, Nazmul Rahmani, and Arshad Ahmad. Degradation modelling and reliability analysis of pem electrolyzer. *International Journal of Hydrogen Energy*, 2023.

[30] PlanEnergi. Upgrading of biogas to biomethane with the addition of hydrogen from electrolysis, 2017. URL `https://futuregas.dk/wp-content/uploads/2018/06/FutureGas-WP1-Deliverable-1.1.1.-Technologies-and-status-of-methanation-of-biogas-2017_Final.pdf`.

[31] Lydia Rachbauer, Gregor Voitl, Günther Bochmann, and Werner Fuchs. Biological biogas upgrading capacity of a hydrogenotrophic community in a trickle-bed reactor. *Applied Energy*, 180:483–490, 2016.

[32] Swellam W Sharshir, Abanob Joseph, Mamoun M Elsayad, Ahmad A Tareemi, AW Kandeal, and Mohamed R Elkadeem. A review of recent advances in alkaline electrolyzer for green hydrogen production: Performance improvement and applications. *International Journal of Hydrogen Energy*, 2023.

[33] Michal Sposob, Radziah Wahid, and Keno Fischer. Ex-situ biological co 2 methanation using trickle bed reactor: review and recent advances. *Reviews in Environmental Science and Bio/Technology*, 20:1087–1102, 2021.

[34] Ajay Thapa, Hongmok Jo, Uijeong Han, and Si-Kyung Cho. Ex-situ biomethanation for co2 valorization: State of the art, recent advances, challenges, and future prospective. *Biotechnology Advances*, page 108218, 2023.

[35] Martin Thema, Tobias Weidlich, Manuel Hörl, Annett Bellack, Friedemann Mörs, Florian Hackl, Matthias Kohlmayer, Jasmin Gleich, Carsten Stabenau, Thomas Trabold, et al. Biological co2-methanation: an approach to standardization. *Energies*, 12(9):1670, 2019.

[36] Matteo Tommasi, Simge Naz Degerli, Gianguido Ramis, and Ilenia Rossetti. Advancements in co2 methanation: A comprehensive review of catalysis, reactor design and process optimization. *Chemical Engineering Research and Design*, 2023.

[37] Panagiotis Tsapekos, Merlin Alvarado-Morales, and Irini Angelidaki. H2 competition between homoacetogenic bacteria and methanogenic archaea during biomethanation from a combined experimental-modelling approach. *Journal of Environmental Chemical Engineering*, 10(2):107281, 2022.

[38] MA Voelklein, Davis Rusmanis, and JD Murphy. Biological methanation: Strategies for in-situ and ex-situ upgrading in anaerobic digestion. *Applied Energy*, 235:1061–1071, 2019.

[39] Wen Wang, Li Xie, Gang Luo, Qi Zhou, and Irini Angelidaki. Performance and microbial community analysis of the anaerobic reactor with coke oven gas biomethanation and in situ biogas upgrading. *Bioresource technology*, 146:234–239, 2013.

[40] Jana Zabranska and Dana Pokorna. Bioconversion of carbon dioxide to methane using hydrogen and hydrogenotrophic methanogens. *Biotechnology advances*, 36(3):707–720, 2018.